ULTRASONIC CAVITATION THRESHOLD MEASUREMENTS IN AN ANECHOIC TANK

By E. V. Shalis

Technical Memorandum
File No. TM 663.2231-07
June 27, 1968
Contract NOw 65-0123-d
Copy No. 6

The Pennsylvania State University
Institute for Science and Engineering
ORDNANCE RESEARCH LABORATORY
University Park, Pennsylvania

NAVY DEPARTMENT · NAVAL ORDNANCE SYSTEMS COMMAND

Abstract: Acoustic cavitation was induced in an anechoic tank at frequencies of 31.8 and 41.3 kHz. The electrical resistance, reactance and impedance of a tonpilz transducer was measured at various transducer voltages before and after cavitation. The appearance of gas and vapor bubbles on the face of the transducer during cavitation was indicated by large changes in measurements made on the input side of the transducer. The projector was linear over the entire transducer voltage range covered.

The spectrum of the first five harmonics was measured. The appearance of the second harmonic proved to be the most sensitive means of detecting the onset of cavitation. The following appeared after cavitation inception: 1) The third, fourth, and fifth harmonic, 2) The subharmonics, and 3) The wide-band noise.

* * *

This thesis was written on research work performed under the direction of Professor E. J. Skudrzyk in the Department of Physics under E/F Account 663.

TABLE OF CONTENTS

LIST OF FIGURES

LIST OF FIGURES

LIST OF FIGURES

LIST OF FIGURES

LIST OF SYMBOLS

E_1	Fundamental voltage amplitude
E_2	Second harmonic voltage amplitude
E_3	Third harmonic voltage amplitude
E_{oc}	Open circuit voltage
M_s	Free-field voltage sensitivity
P_A	Driving force amplitude
P_c	Pressure within cavity
$P_g(R_o)$	Gas pressure inside bubble at zero time
$P_g(R)$	Gas pressure inside bubble at any time
P_i	Incident pressure amplitude
P_r	Reflected pressure amplitude
P_L	Static liquid pressure
P_v	Vapor pressure
P_∞	Pressure in the liquid at large distances from the cavity wall
r	Distance between projector and hydrophone
R'	Reflection coefficient
R	Cavity radius
$\overline{R}$	Average cavity radius
$\dot{R}$	Velocity of cavity wall
$\ddot{R}$	Acceleration of cavity wall

$\|R\|$	Electrical resistance of transducer
R_c	Critical cavity radius
R_{max}	Maximum size of cavity
THD	Total harmonic distortion
v_s	Velocity of sound
v	Volts
μv	Microvolts
$\overline{Z}$	Complex electrical impedance
α	Absorption coefficient
δ	Phase angle
γ	Specific heat ratio
σ	Surface tension pressure
ω	Angular frequency
ω_f	Characteristic frequency
ω_o	Linear resonant frequency

CHAPTER I

INTRODUCTION

1.1 Origin and Importance of the Investigation

Cavitation is related to the growth and the collapse of voids in liquids. There exist two distinct types of cavitation. Gaseous cavitation is a degassing process. It occurs at low driving amplitudes and the bubbles grow through rectified diffusion of gases coming out of solution.[1] The gas bubbles that result will remain in the liquid even when the driving force is turned off and will eventually rise to the surface. Gaseous cavitation does not emit a sound spectrum and may exist simultaneously with vaporous cavitation. Vaporous cavitation begins at higher amplitudes and is characterized by intense bubble motion and sharp snapping sounds. One can see streaming bubbles either moving in a random way or being trapped in the acoustic field.

Vaporous cavitation will occur in gas saturated liquids. Whenever it exists in pure liquids, it is called true cavitation. Confusion usually arises when the different forms of cavitation are not distinguished.

This investigation will describe the appearance of vaporous cavitation. Cavitation is an extremely nonlinear phenomenon. The changes in the system during cavitation will be investigated at increasing sound intensities.

The occurrence of cavitation will depend on many variables, such as:

1. Frequency,
2. Duration and type of driving signal,
3. Properties of the cavitating medium,
4. Gas content,
5. Concentration and size of the gas nuclei,
6. Ambient pressure,
7. Liquid temperature, and
8. Boundary conditions of the medium.

Various investigators have been able to control a few of these variables and have measured the pressure levels needed to cavitate the liquid. The size and the concentration of gas bubbles present in the liquid and their effect on cavitation has been measured by Noltingk.[2] He measured the type of bubbles present by noting the increased absorption that occurs at the resonant frequencies of the bubbles.

Sette has noted that nuclei will influence cavitation since their presence indicates weaknesses in the liquid.[3] These nuclei may be solid dust particles or gas bubbles that exist on the transducer face.

Esche has observed a line spectrum superimposed upon a wide-band noise at cavitation intensities. The appearance of the wide-band noise would imply a pronounced effect that could be used to distinguish between cavitating and non-cavitating intensities. The continuous wide-band noise is due to the collapse of the bubbles when they are subjected to a time dependent force.[4] Esche suggested that the line spectra consisting of the driving frequency and its harmonics and subharmonics are due to the nonlinear oscillations of the bubbles. Holak has measured cavitation spectra in a reflective tank.[5] However, a search through the literature has not revealed a simple measure of the onset of cavitation. In this investigation, harmonic distortion measurements will be used to determine when cavitation begins.

1.2 Statement of the Problem

It appears difficult to measure a cavitation threshold when so many parameters influence the result. Numerous investigators have used the following techniques to determine cavitation inception:

1. The appearance of cavities in the liquid,
2. The growth of cavities to a certain size, and
3. The appearance of wide-band noise as the power to the transducer is increased.

Cavitation is caused by the breaking up of the liquid in the under-pressure phase. Small gas-filled cavities are formed that grow in the under-pressure phase and collapse implosively in the pressure phase. Because the formation and collapse of these cavities is triggered by every second half-wave of pressure, cavitation leads to a strong second harmonic of the exciting frequency. The appearance of this second harmonic is an extremely sensitive means to discover the onset of cavitation. The typical cavitation noise occurs only when the intensity is far above the threshold of cavitation. The statistical nature of the generation of the bubbles leads to higher harmonics and subharmonics which are normally construed to indicate the presence of cavitation.

Thus, the onset of cavitation is indicated with extremely high accuracy by the appearance of the second harmonic of the exciting frequency. We will define the onset of cavitation as the generation of the second harmonic of the exciting frequency. Everything else reported in the literature occurs at a greater input power. The following will appear at larger pressures than those needed to generate the second harmonic:

1. The third, fourth, and fifth harmonics,
2. The subharmonics, and
3. The wide-band noise.

The onset of cavitation will be detected by noting the appearance of the second harmonic on a spectrum analyzer. This method is more sensitive than noting the total distortion as seen on an oscilloscope. The minimum pressure level required to raise the level of the second harmonic to within 15 dB of the fundamental will be defined as the cavitation threshold. No other criteria will be applied.

We shall concentrate exclusively on cavitation in this investigation. Second harmonic levels due to finite amplitude distortion are usually 50 dB down from the fundamental signal at projector-receiver separations of 10 feet.[6] The levels of the second harmonic due to cavitation were within 20 dB of the fundamental signal at projector-receiver separations of 15 inches. Typical input powers of 0.7 watts/cm^2 are required to cavitate tap water Thus, the distortion due to the nonlinearity of the medium is negligible for small distances from the source and low driving amplitudes.

The response of the projector used in this investigation was linear up to input powers of a few hundred watts. Having a linear medium and a transducer with a linear response allows us to concentrate exclusively on the nonlinearities due to cavitation.

The following measurements will be made of the effects of cavitation on our system:

1. Measurement of the change in the properties of the transducer at cavitation intensities. It is expected that cavitation on the face of the transducer will unload the transducer due to the appearance of gas and vapor bubbles on its face. The impedance, reactance and resistance on the input side of the transducer will change during the onset of cavitation as detected by the appearance of the second harmonic.
2. The total harmonic distortion increases at cavitation. This includes distortion due to the second and higher harmonics and also due to the subharmonics. The distortion will be primarily second harmonic. The total harmonic distortion will be measured before and after cavitation.
3. The line spectrum consisting of the second through the fifth harmonics will be investigated at low and high intensities. The change in the pressure level of this line spectrum will be noted at the onset of cavitation and also for very intense cavitation where the wide-band noise can be detected.
4. As a preliminary part of the investigation, the amount of distortion introduced by the boundaries of the container will be measured. Free-field-type conditions are necessary for repeatable data.

1.3 Method of the Investigation

Previous authors have investigated cavitation in small volume enclosures. The results have been strongly frequency dependent due to the dimensions of the medium. Small enclosures lead to standing wave patterns that focus at one or two main resonant points in the medium. The limitation of taking data at only a few points is highly restrictive. We have built an anechoic tank that presents semifree-field-type conditions to our system. This should reduce the dependence on boundary conditions and prevent random cancellation of the cavitation line spectrum.

The anechoic tests were performed at the Ordnance Research Laboratory. Transmission and absorption measurements over a frequency range of 30 kHz to 120 kHz were made with a directional source when the tank was filled with tap water. The results are compared with those obtained in a highly reflective 5-1/2 gallon tank. A tuning circuit was built to smooth out the frequency response of the QP-1 transducer source.

The Atlantic Research Corporation Hydrophone, Model LC-5, Serial No. 50, was calibrated at the Black Moshannon Calibration Station. This hydrophone was used throughout the investigation. Free-field voltage response from 0.1 to 0.8 MHz was measured. Receiving directivity patterns for both the horizontal and vertical planes were obtained at 0.5, 0.6, 0.7, 0.8, 0.9, and

1.0 MHz. Cavitation was induced at 31.8 and 41.3 kHz with an ORL 4X-47 tonpilz transducer. Constant voltage transmission response at one yard and impedance plots in both water and air were obtained.

The distortion introduced by the input side of the transducer was checked by making total harmonic distortion measurements of the Hewlett Packard 208 oscillator and the 200-watt McIntosh power amplifier. A frequency response at intermediate and full power output was also obtained.

The behavior of the nonsymmetrically loaded transducer during cavitation was estimated by noting how the impedance changed as a function of power input. The appearance of weak points in the liquid would effectively unload the transducer and limit the amount of power that could be radiated into the liquid. The amount of power needed to unload the transducer was compared with the power that was necessary to cause the liquid to cavitate.

Cavitation was defined as the appearance of the second harmonic of the exciting frequency. At low intensities, the level of the second harmonic was too low to be measured. The distortion analyzer and the SKL band-pass filter were used to eliminate the fundamental and allow the level of the harmonics to be raised without overloading the analyzer. Cavitation was said to exist whenever the second harmonic was 15 dB down from the fundamental. This served as the threshold criterion.

CHAPTER II

DESCRIPTION OF THE EQUIPMENT

2.1 The Anechoic Tank

The investigation was conducted at the Water Tunnel complex of the Ordnance Research Laboratory at The Pennsylvania State University in an anechoic tank built by the author. The anechoic tank is shown in Figure 2.1. The tank was designed to reduce standing waves. The volume of the tank was 24 cubic feet with the dimensions being four feet by three feet by two feet. The water capacity was 1500 lbw. The tank was reinforced with two-inch by four-inch marine plywood. Two-inch triangular-shaped fir wedges were glued to the sides of the tank. The wedges on opposite walls were perpendicular to each other. All faces of the tank, including the bottom and the top, were lined accordingly. The tank was allowed to soak for a period of two months before data was taken so that the acoustic absorption of the wedges would increase. Measurements of absorption coefficients were made with and without the top on. Surface reflections were further lowered by completely filling the tank to the top. The top wedges were accordingly well-soaked and the water-air interface was eliminated. The anechoic tank was made air tight

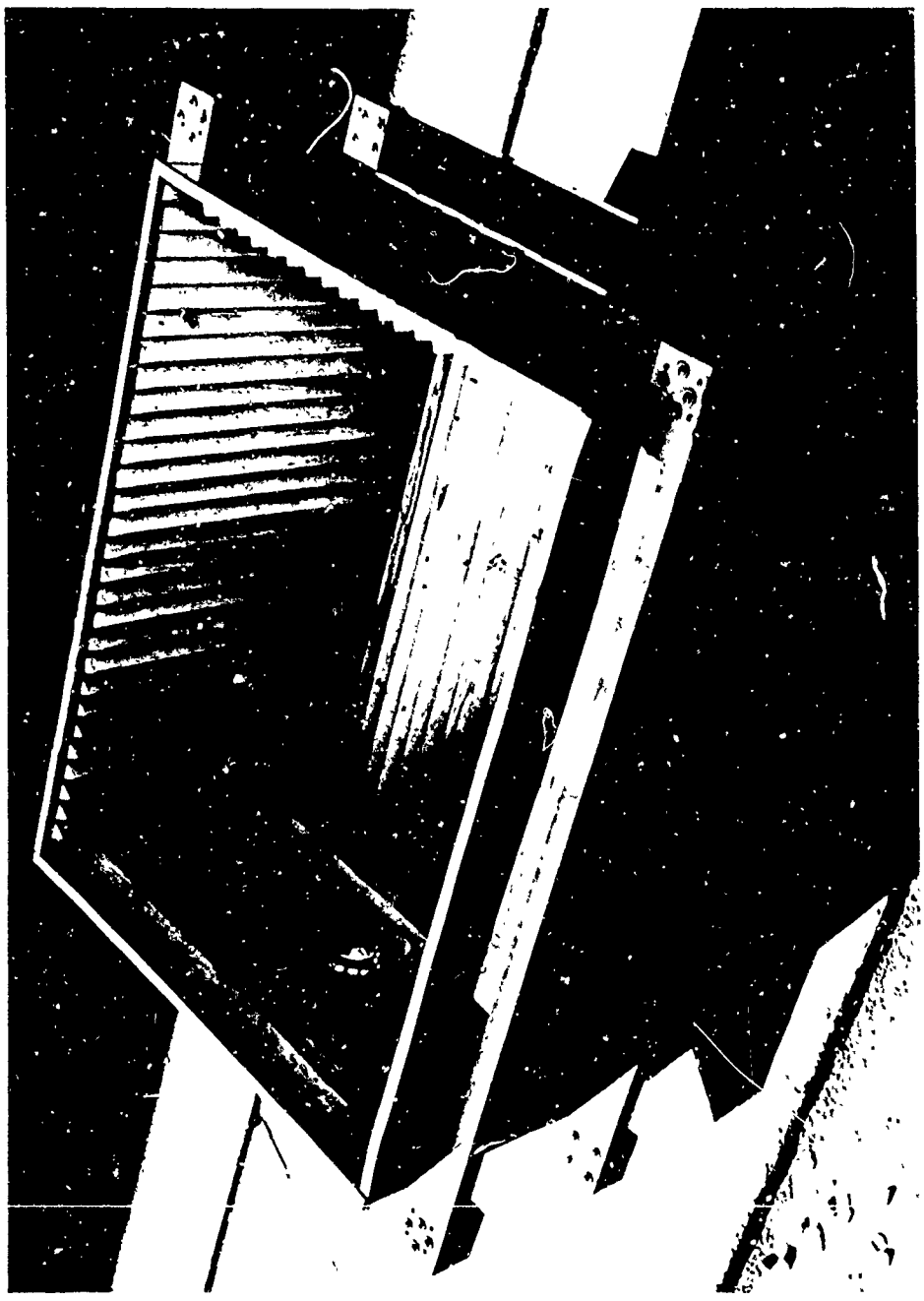

Figure 2.1. Anechoic Tank

and openings for a circulation pump and transmission lines were provided. The tank contained no metal parts other than the screws that held the optical flats on opposite sides of the tank. The optical flats were installed to provide for future light-sound interaction measurements. They served as openings for field illumination by a Tensor Model 7200 light source. The anechoic tank was placed on the floor for further bottom support and was cleaned periodically. Although ideal conditions for measurement in an infinite medium could not be obtained, the absorption coefficient measurements showed that the tank produced semi-free-field conditions.

Two techniques were used to determine how much distortion of the acoustic field was produced by the tank. Pure-tone transmission data was taken with an Ordnance Research Laboratory Type QP-1 transducer. This transducer was selected for both transmission and reflection measurements due to its flat frequency response curve over the range of 20 to 120 kHz. The frequency response of the QP-1 transducer at 10 and 20 inches away from the source is shown in Figure 2.2. The effect of the standing waves is very noticeable at a transducer-hydrophone separation of 20 inches. A tuning network was used to make the response curve of the transducer more uniform. This inverse network is shown in Figure 2.3.

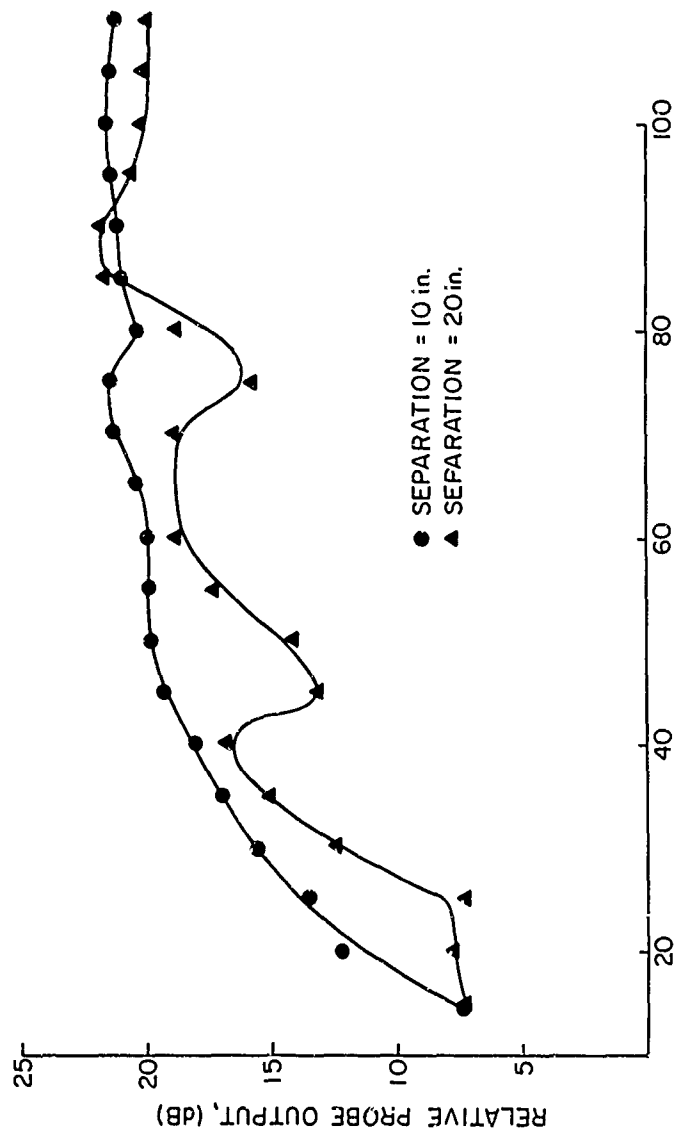

Figure 2.2. Frequency Response of QP-1 Transducer at Two Transducer-Hydrophone Separations

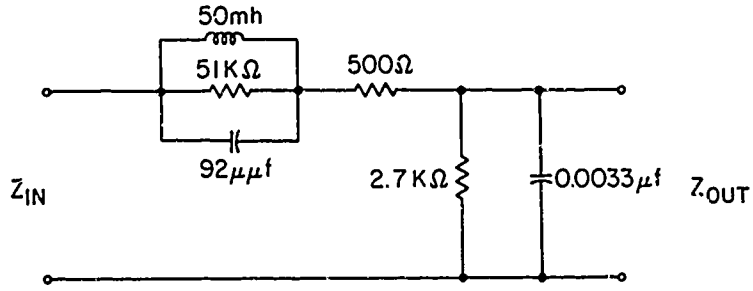

Figure 2.3. The Transducer Inverse Network

The improved response curve at 10 and 20 inches separation is shown in Figure 2.4.

The LC-5 pressure probe was separated from the transducer in two-inch intervals during the $1/r^2$ transmission tests. The frequency was held constant as the probe was moved over the range of separation from 4 to 30 inches. The results in Figure 2.5 show that $1/r^2$ behavior will not exist in the near field. The 6 dB per octave straight line is drawn using the 10-inch separation as a reference.

2.2 The Transducers

The following three transducers were used to induce cavitation in the anechoic tank:

1. EX-2 tonpilz,
2. 4X-47 tonpilz, and
3. Barium titanate cylinders.

Only the 4X-47 transducer delivered sufficient acoustic power in the frequency range of 10 to 60 kHz. A picture and a schematic diagram of the projector are shown in Figures 2.6 and 2.7. The delivered acoustic power was further increased by using a circuit tuning coil consisting of inductances from 1 to 19 millihenries.

The four-element, oil-filled 4X-47 experimental transducer was chosen for the investigation because of the following projector characteristics:

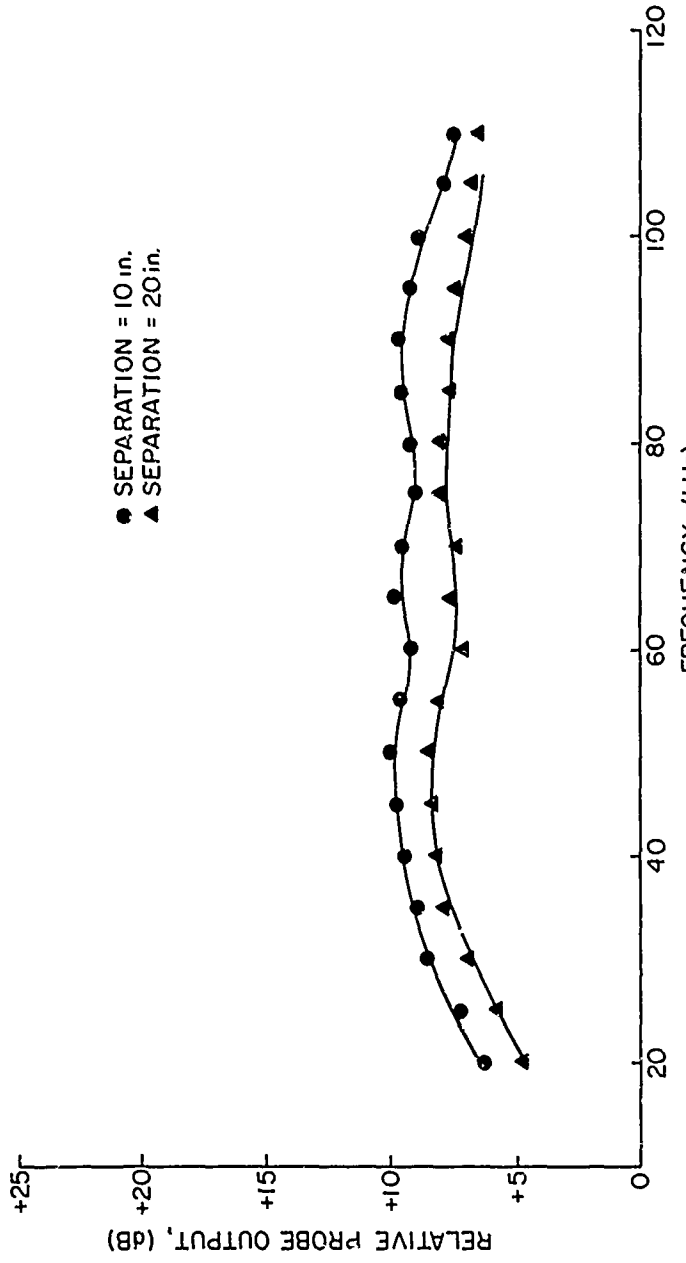

Figure 2.4. Frequency Response of QP-1 Transducer with Inverse Network at Two Transducer-Hydrophone Separations

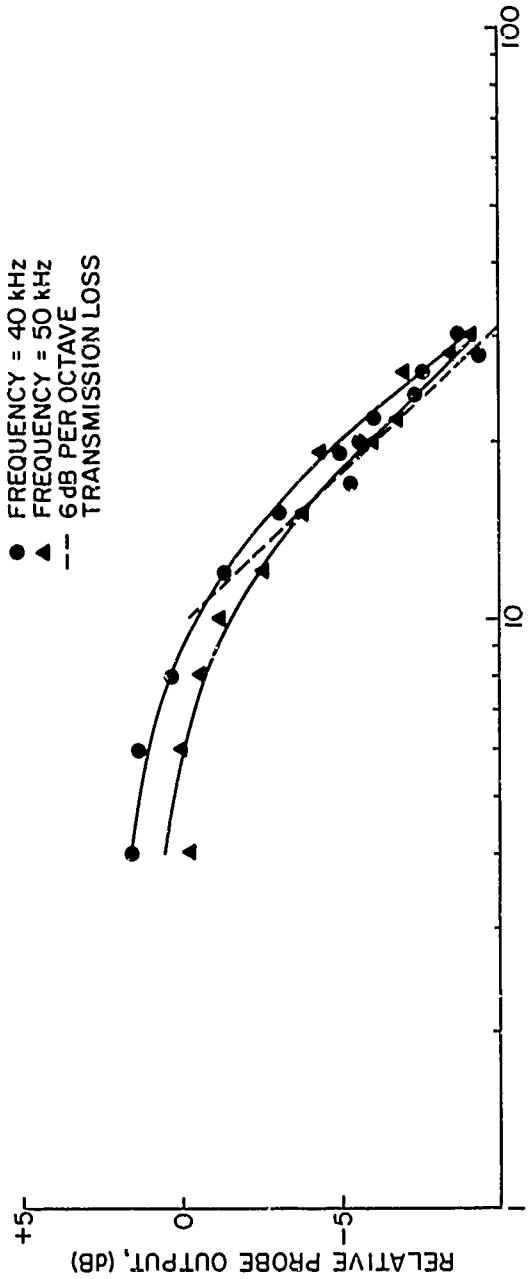

Figure 2.5. Output of Pressure Probe at Two Frequencies for Different Projector-Receiver Separations

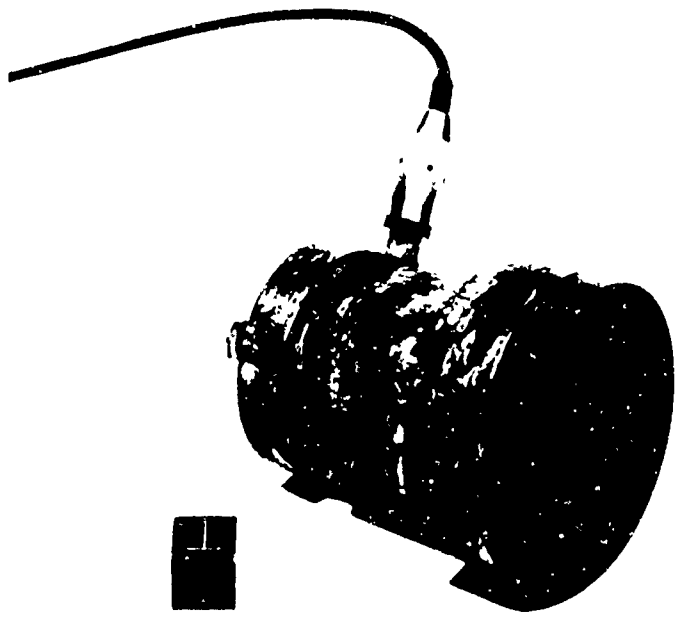

Figure 2.6. Four-Element 4X-47 Transducer

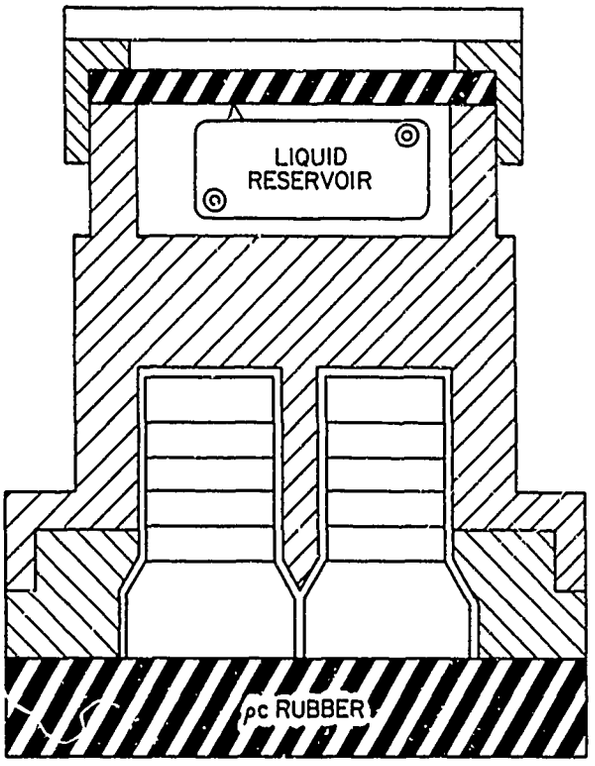

Figure 2.7. Schematic Diagram of 4X-47 Transducer

1. High power factor,
2. High efficiency,
3. Uniform directionality response, and
4. Good pattern with good front-to-back ratio.

The elements are separated by one-sixteenth inch of fluid. Low ρc rubber was used as part of the housing and provided good coupling with the water. The efficiency of the transducer was 70 percent.

Impedance and admittance plots were obtained in the anechoic tank over a 10 to 60 kHz range. The Dranetz Vector Admittance-Impedance Meter was used and the results are shown in Figure 2.8. Frequencies of 31.8 and 41.3 kHz were chosen on the basis of information obtained from the admittance circle.

Figure 2.9 shows the constant voltage transmission response at one yard for the 4X-47 transducer. The response is given in dB reference one microbar rms per volt and is fairly flat in the 28 to 48 kHz region.

2.3 The Atlantic Research Model LC-5 Pressure Probe

The investigation required a small hydrophone with a good response up to 1 MHz. The four-inch long LC-5 hydrophone was used throughout the investigation because of its ruggedness and flat response at low and high frequencies. The sensing element is lead zirconate titanate. A waterproof neoprene sheath is bonded to the element to provide good coupling with the medium.

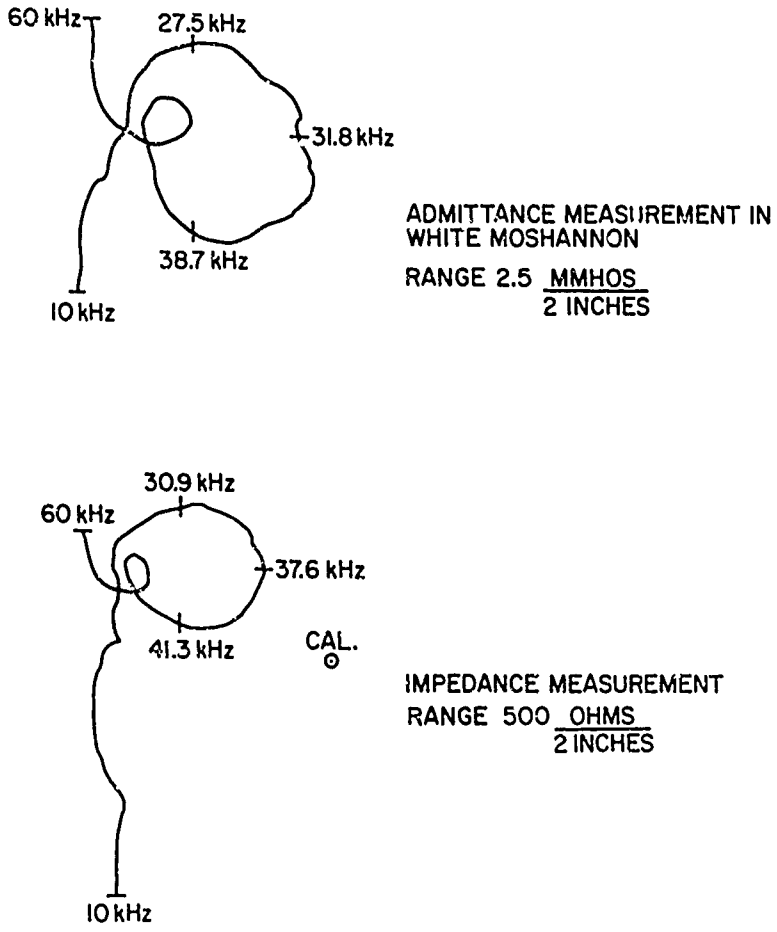

Figure 2.8. Admittance and Impedance Circles of the 4X-47 Transducer

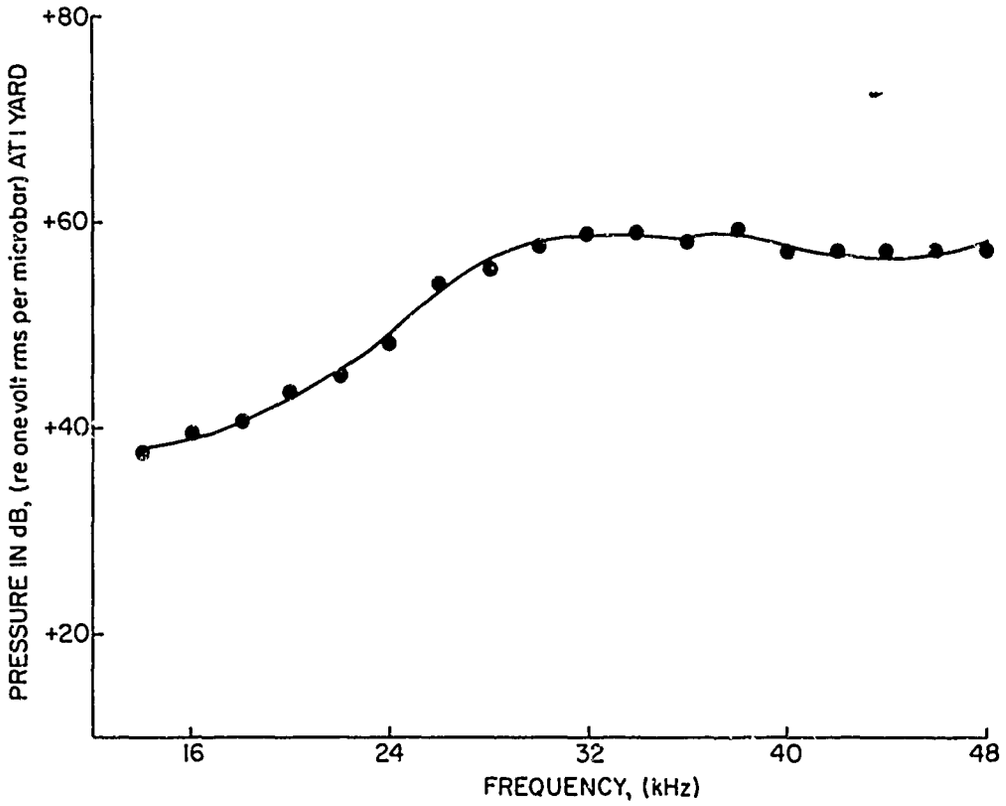

Figure 2.9. Constant Voltage Transmission Response at One Yard for the 4X-47 Transducer

The capacitance of the LC-5 hydrophone is 150 μμf. The maximum allowable sound pressure is 131 dB (re 0.0002 dyne/cm^2) from 0.1 to 0.7 MHz. A picture of the probe is shown in Figure 2.10. In order to insure accuracy of the threshold pressure, the hydrophone was calibrated by the free-field reciprocity method. Receiving patterns from 0.5 to 1.0 MHz in the horizontal and vertical planes were obtained at the Black Moshannon Calibration Station of the Ordnance Research Laboratory.

The theory of free-field reciprocity methods are discussed by Albers and Holak.[7, 5] Free-field voltage sensitivity of a hydrophone is defined as:

$$M_s = \frac{\text{open-circuit voltage}}{\text{free-field sound pressure}}$$

or

$$M_s = \frac{E_{oc}}{P_i} .$$

The free-field voltage response of the LC-5 probe is given in Figure 2.11. The response is flat at approximately -137 dB per 1 volt per μbar.

Receiving directivity patterns of the LC-5 probe were measured at frequencies of 0.5, 0.6, 0.7, 0.8, 0.9, and 1.0 MHz for both the horizontal and vertical planes. The directivity patterns measure the response of the probe as a function of angle at a particular frequency. The NRL-USRD Type E-8, Serial No. 53, projector was used with a six-foot separation between

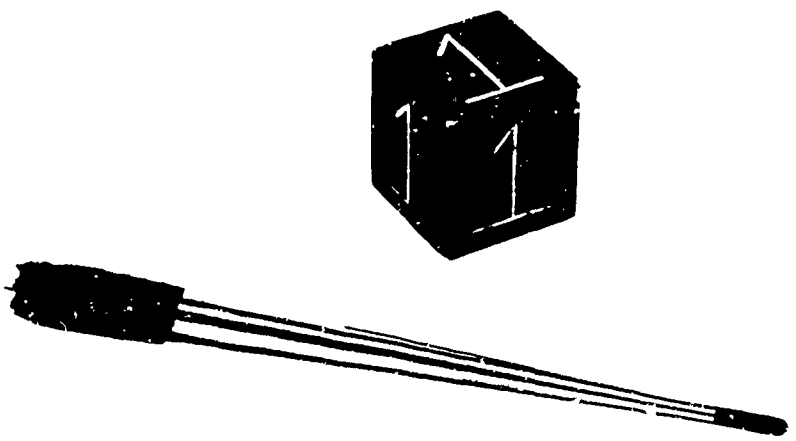

Figure 2.10. Atlantic Research LC-5 Pressure Probe

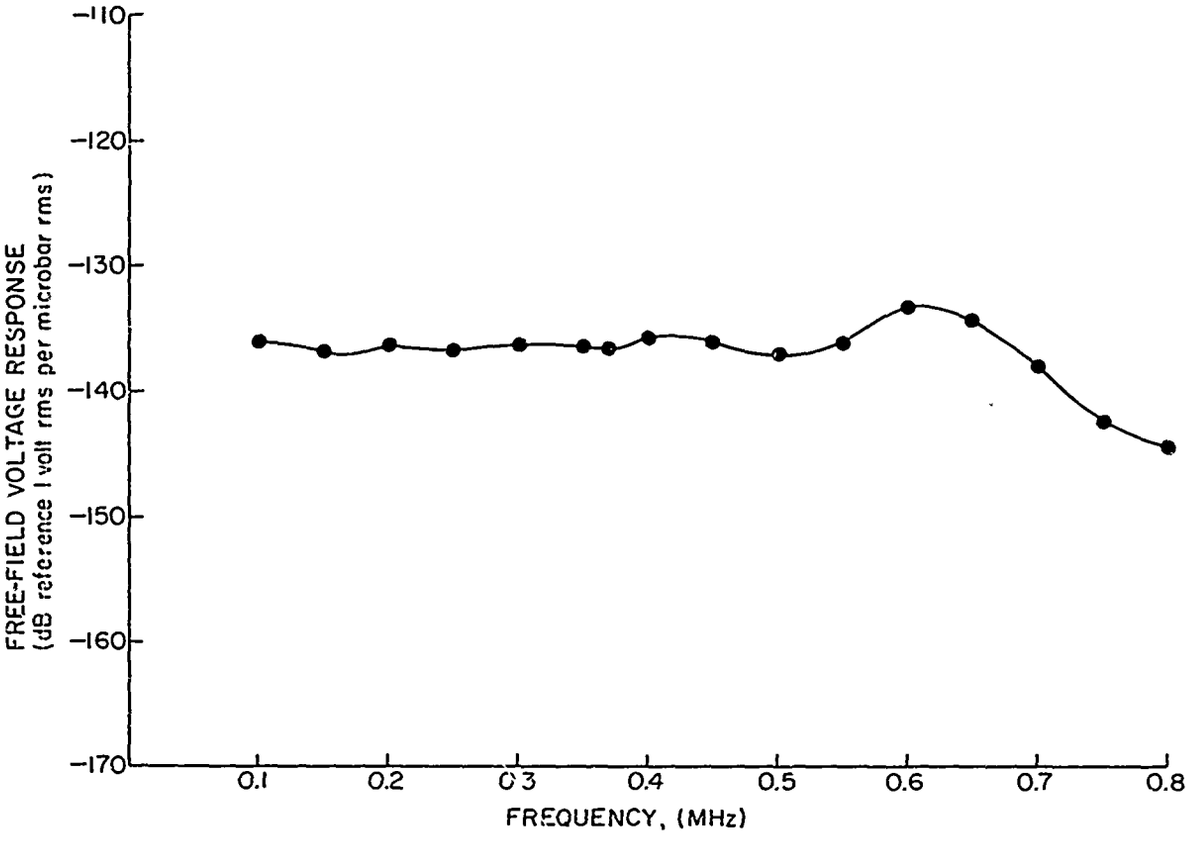

Figure 2.11. Calibration of LC-5 Pressure Probe

projector and receiver at a seven-foot immersion depth. Pulses of 0.1 ms and 10 ms repetition rate were used to distinguish between direct and reflected signals. A typical pattern in the horizontal plane at 0.5 MHz is shown in Figure 2.12. The horizontal plane orientation was used throughout the investigation.

2.4 The Spectrum Analyzer

A calibrated Panoramic Singer Universal Spectrum Analyzer, Model TA-2, with Ultrasonic Module was used in the spectrum study to analyze the signals received by the LC-5 hydrophone. The Panoramic displayed signal level versus frequency from 100 Hz to 700 kHz. Since the frequency range of 10 to 300 kHz was investigated, the frequency range of the Panoramic was greater than necessary. Signals of 3 μv could be measured by the Panoramic and a preamplifier was used to increase signal amplitude. The high impedance Panoramic displayed harmonics 50 dB down from the fundamental. Instantaneous input signals were limited to less than 100 volts. The amplitude response was ±0.5 dB from 100 Hz to 500 kHz whenever the instantaneous input signal was less than 100 volts. Input and intermediate frequency attenuators were used to prevent overdriving the unit.

2.5 The Electronic Apparatus

The apparatus used in the study is shown in Figure 2.13, and a block diagram of the equipment is shown in Figure 2.14. A Tektronix current probe was used to measure current to the

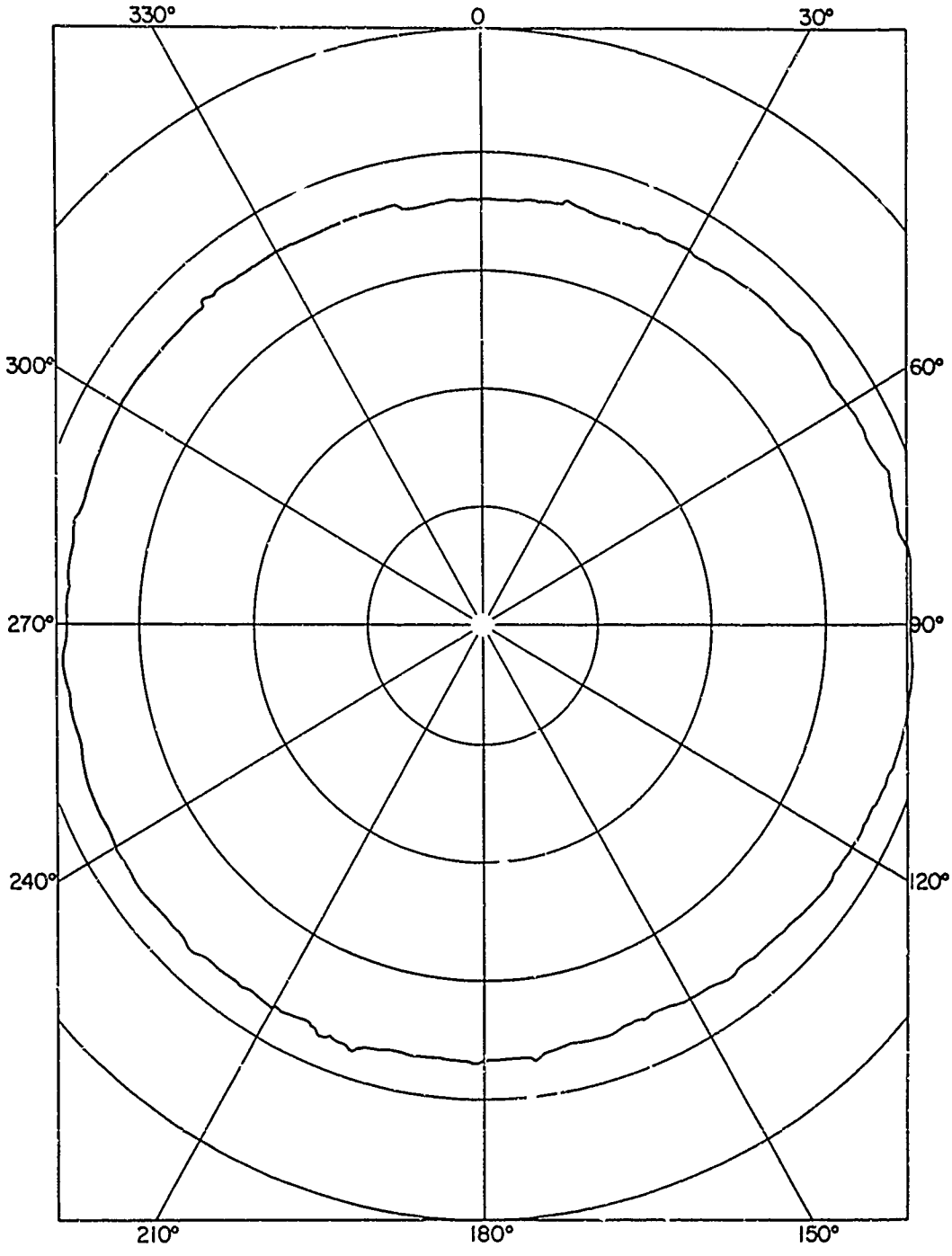

Figure 2.12. Receiving Pattern in Horizontal Plane at 0.5 MHz

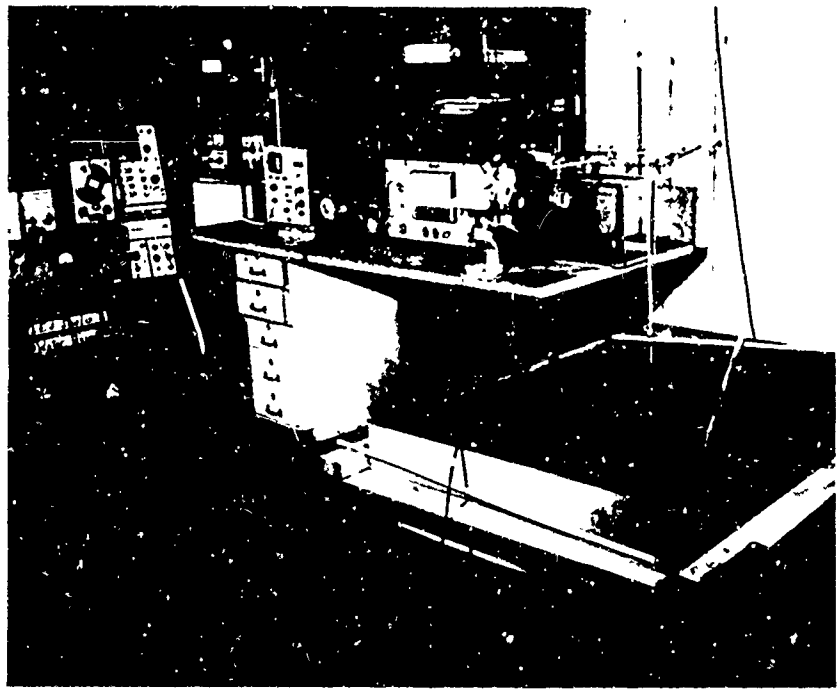

Figure 2.13. Electronic Apparatus

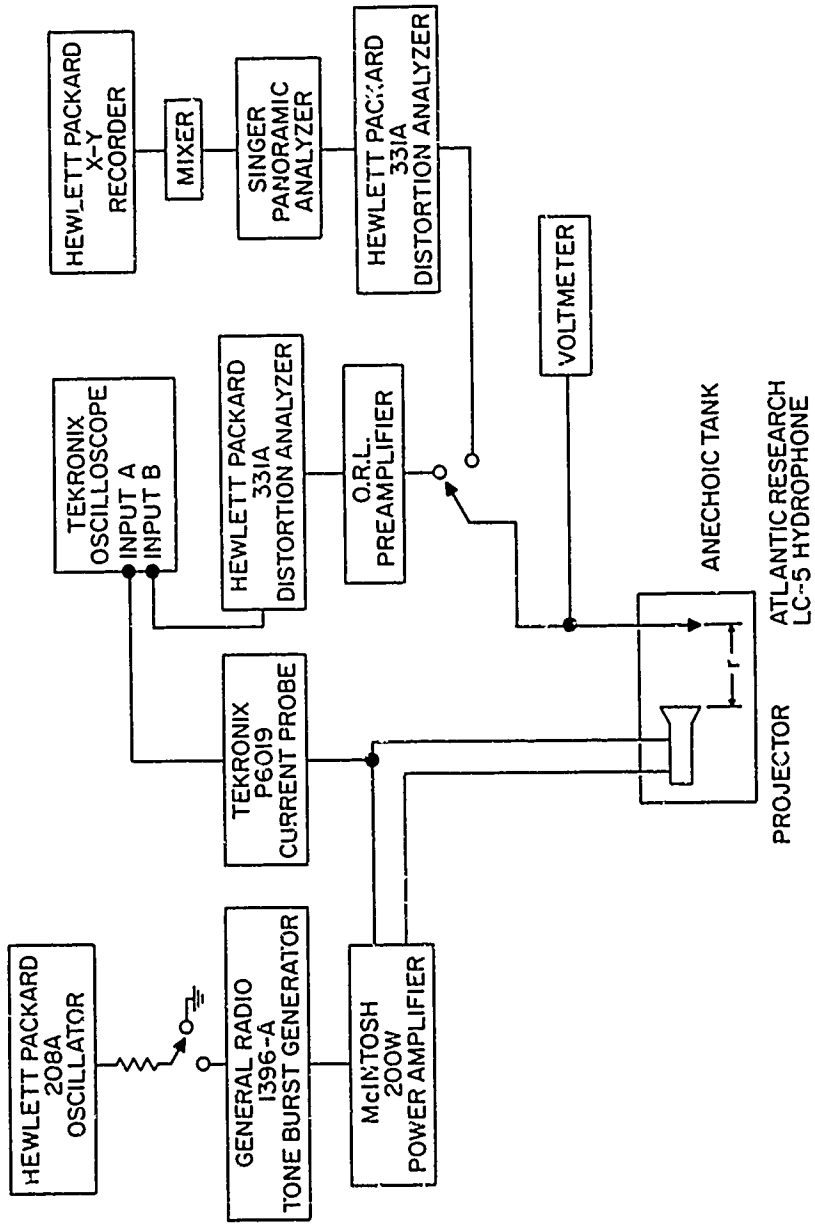

Figure 2.14. Electronic Apparatus: Block Diagram

projector. The probe was placed around the conductor and the resulting current waveform was displayed on the Tektronix oscilloscope. Circuit loading was prevented by clamping the probe to the ground end of the component lead. The high frequency response was greater than 60 MHz.

Frequency response and instrument distortion of the detection circuit was measured over a 10 to 110 kHz range. The oscillator response was flat as expected. The response of the McIntosh 200-watt power amplifier into a 100 ohm resistive load at full and intermediate output is shown in Figure 2.15. Only a few frequencies were used at full output due to resistor heating. The total harmonic distortion of the 200-watt amplifier at intermediate and full output is shown in Figure 2.16. The intermediate range presents an insignificant amount of distortion over frequencies from 10 to 110 kHz. The total harmonic distortion of the ORL preamplifier is presented in Figure 2.17. The distortion of the preamplifier is less than 1.5 percent for frequencies less than 100 kHz. The distortion in the oscillator signal is insignificant as expected.

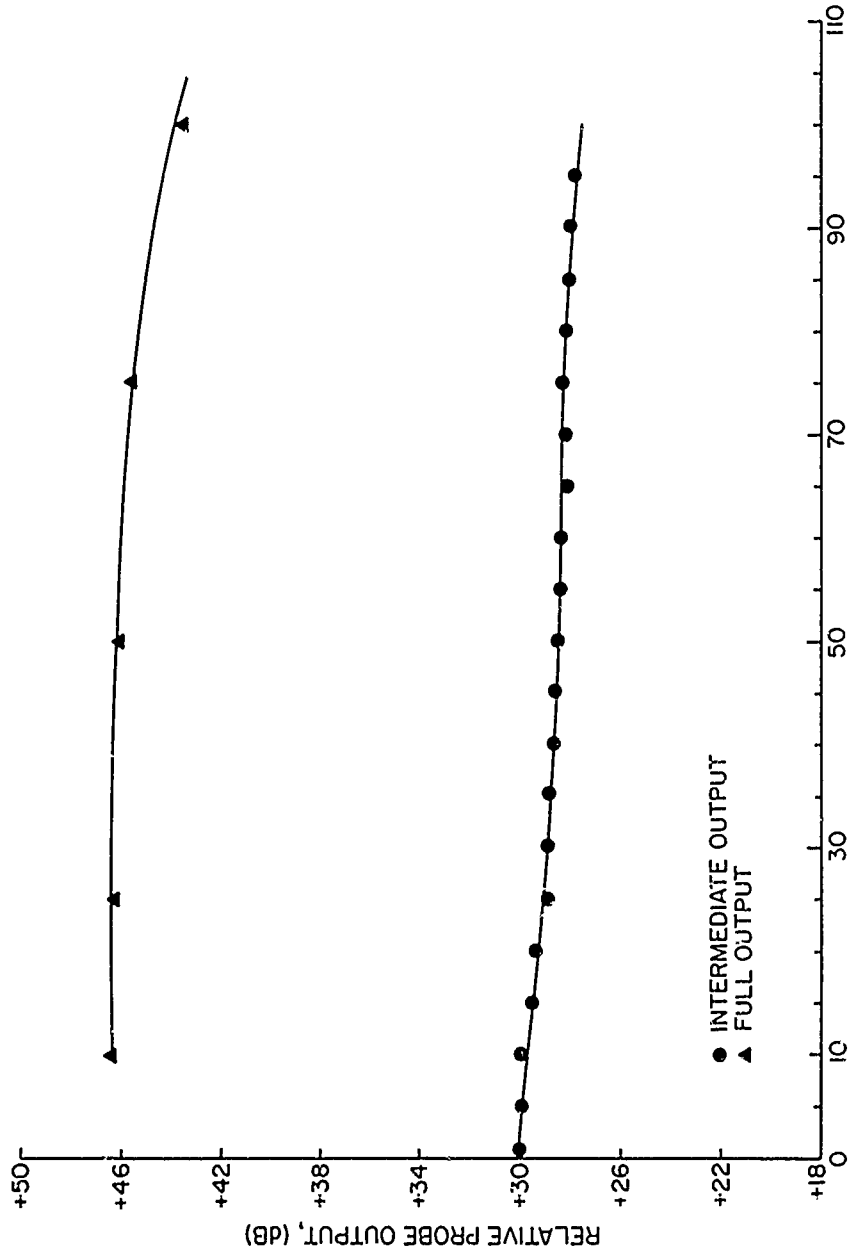

Figure 2.15. Frequency Response of Power Amplifier into a 100 Ohm Resistive Load

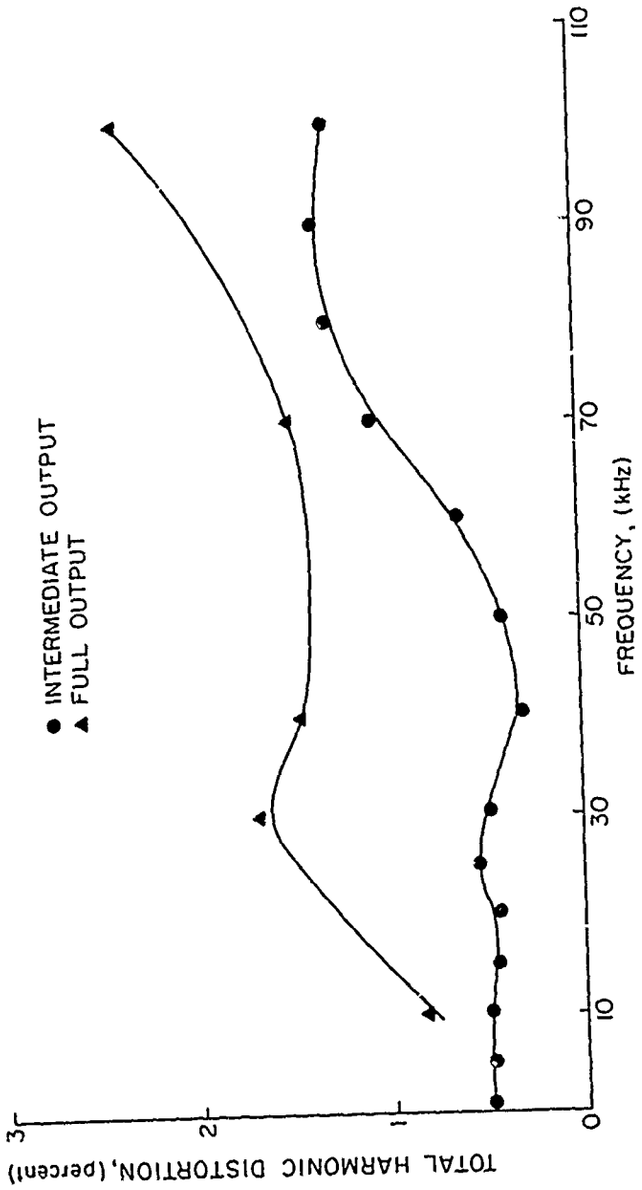

Figure 2.16. Total Harmonic Distortion of the Power Amplifier

Figure 2.17. Total Harmonic Distortion of Preamplifier

CHAPTER III

EXPERIMENTAL PROCEDURE

3.1 History of the Investigation

The investigation began with measurements of total harmonic distortion of signals received by the LC-5 hydrophone before and after the water cavitated in a 5-1/2 gallon fish tank. Cavitation was induced by a cylindrical barium titanate transducer. Pictures of the cavitating medium and the LC-5 hydrophone positioned inside the transducer are shown in Figure 3.1. The pictures were taken with a Nikon Stereoscopic Microscope, Model SMZ-2, using a shutter speed of 1/100 second and Polaroid Type 3000 film. A high intensity stroboscopic light source was used to shorten the exposure time. The data was not repeatable due to standing-wave effects in the undamped tank. The dimensions of the source, the wave length, and the dimensions of the receiver influenced the results. Previous investigators have decreased standing-wave field effects by placing the receiver at a resonant position. This was done in our case by placing the LC-5 hydrophone directly inside the cylinder on its acoustic axis. Distortion measurements made before and after cavitation were again too great to be reliable. It was decided that a free-field medium was needed to obtain accurate data.

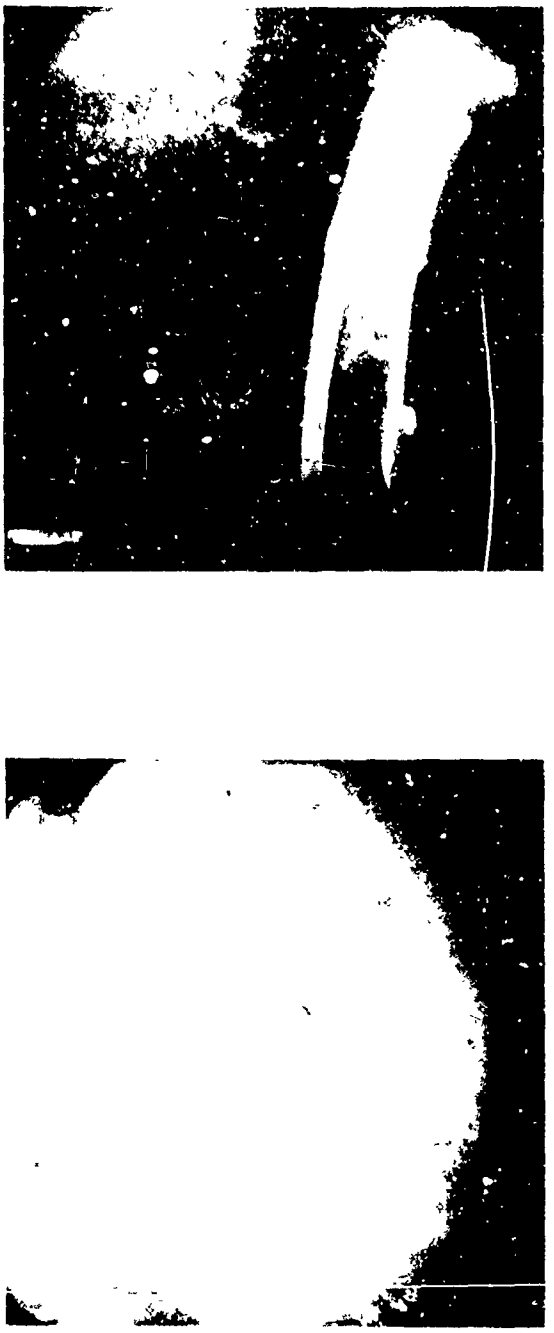

Figure 3.1. Cavitation in the 5-1/2 Gallon Tank

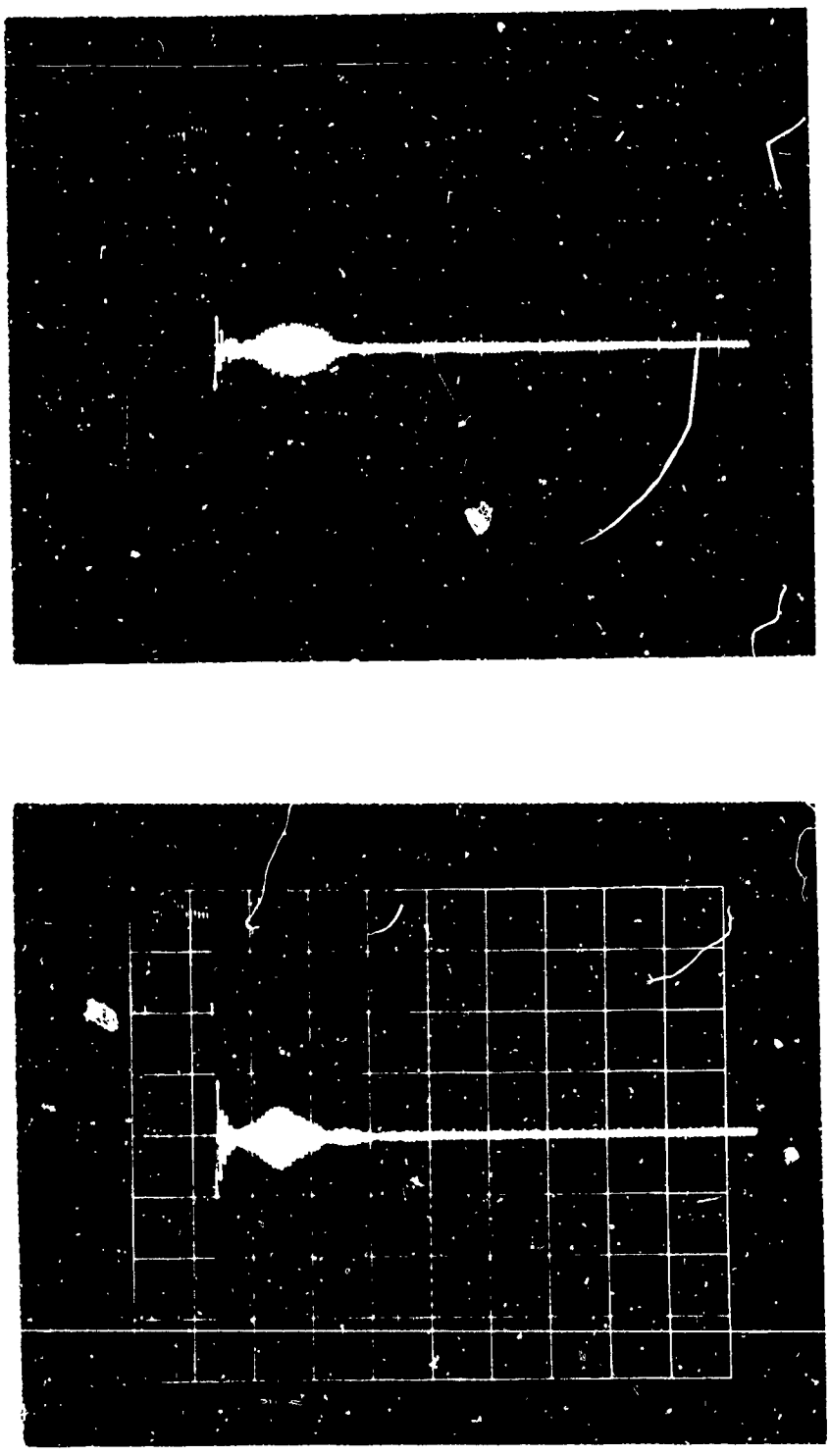

Figure 3.2. Pressure Pulses in the Anechoic Tank for Transducer-Hydrophone Separation of 10 Inches

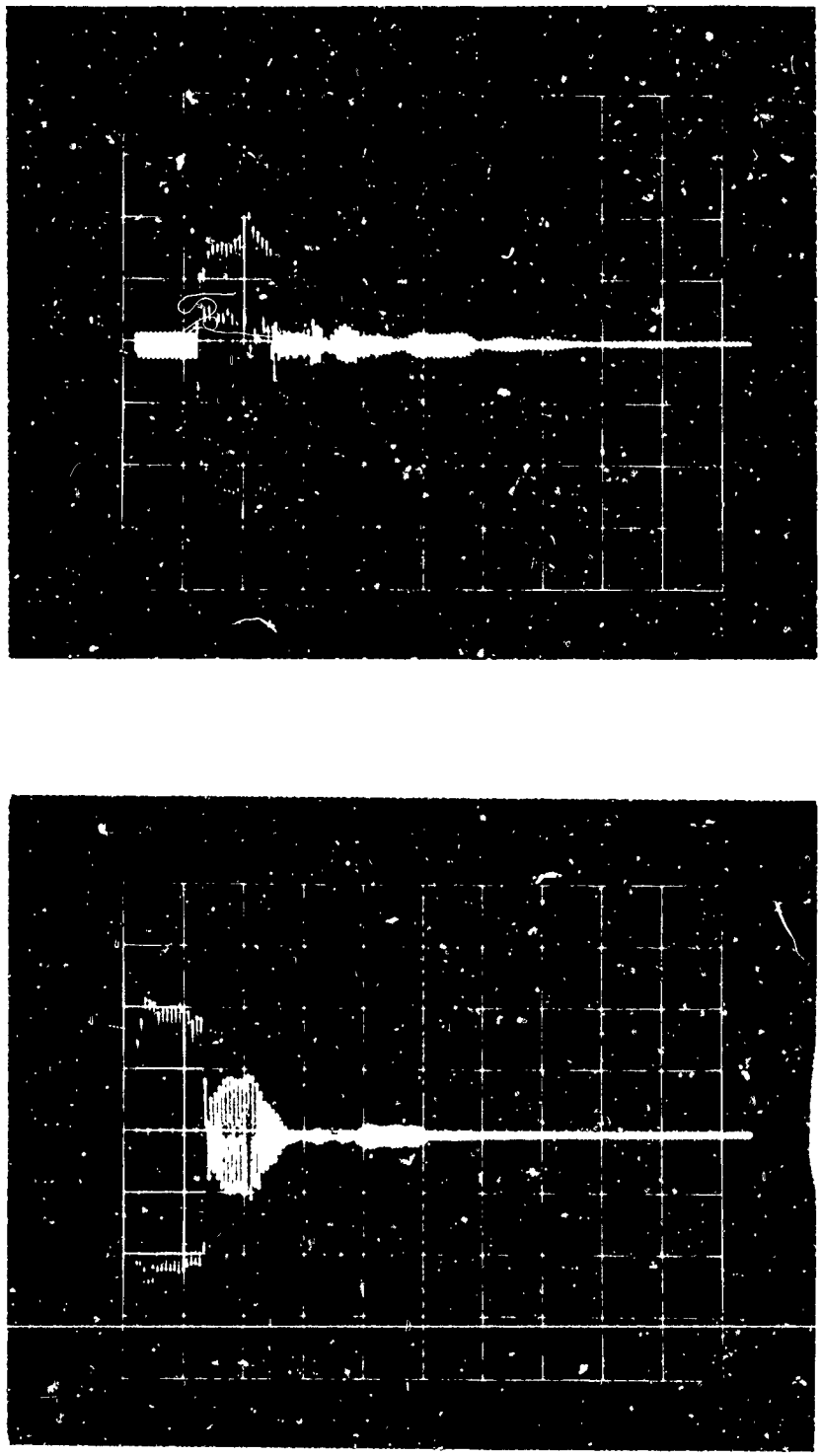

Figure 3.3. Pressure Pulses in the Anechoic Tank for 20-Inch Transducer-Hydrophone Separation

An anechoic tank was built at the Ordnance Research Laboratory. Energy loss measurements were made using pulsed and CW modes. The magnetostrictive QP-1 transducer transmitted short pulses of 4, 16, and 32 cycles with a 10 ms time delay between transmissions. The transmission was further improved by using low driving signals and a nonsymmetrical alignment between receiver and projector.

Absorption measurements were made over a 30 to 100 kHz range maintaining proper triggering between the oscilloscope and the tone burst generator. The LC-5 hydrophone recorded direct and reflected pulses and they were displayed on the oscilloscope. Absorption coefficient α was obtained using:[8]

$$R' = \left(\frac{P_r}{P_i}\right)^2$$

and $$\alpha = 1-R',$$

where P_i is the incident pressure pulse, P_r is the reflected pressure pulse, and R' is the reflection coefficient. The incident pulse was fixed at 1 volt peak to peak to reduce errors in measurement. Figures 3.2 and 3.3 show typical single sweep pulses obtained in the anechoic tank at separations of 10 and 20 inches, respectively. The pulses in Figure 3.2 (a) and 3.3 (a) were taken with the top off. The pulses in

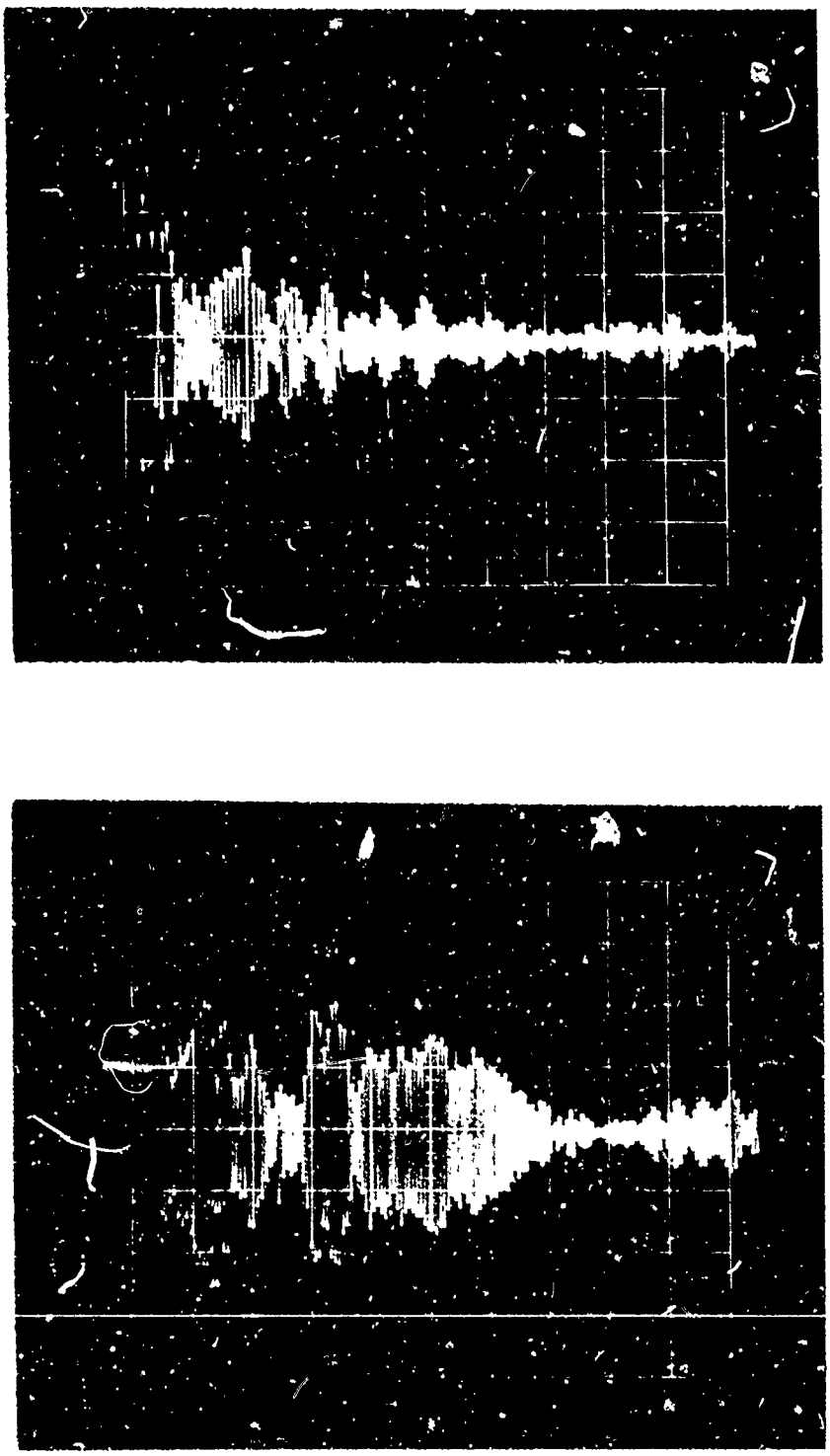

Figure 3.4. Pressure Pulses in the 5-1/2 Gallon Tank

Generally, the procedure was to place the projector at a fixed depth. The resonant frequency of the projector was selected so that spurious signals were not transmitted. Pulses did not repeat when cavitation existed and it became difficult to analyze the distorted waveform visually on the oscilloscope. Figure 3.5 shows some typical cavitation waveforms. Precautions were taken not to overdrive the oscilloscope or the preamplifier. The spread in the data points did not warrant corrections for small bulk temperature and pressure changes. The age and the dissolved air content of the liquid was noted and generally was between 10 to 20 parts per million.

In the spectrum measurements, the high frequency components were analyzed with the Panoramic analyzer before and after cavitation. The 3-1/2 inch square oscilloscope of the wave analyzer was used for quick display of the signal. The output of the analyzer was fed to the Hewlett Packard X-Y recorder. The calibrated 40 dB spread of the X-Y recorder is shown in Figure 3.6. The log amplitude scale was used for signals from 30 to 250 kHz and strong signals were attenuated by the input and I.F. attenuators. The input attenuator decreased signals in 10 dB steps to 100 dB and an additional 20 dB attenuation in 5 dB steps was available with the I.F. attenuator. Continuous adjustment was made on the distortion analyzer to eliminate the driving frequency so that the higher harmonics could be recorded.

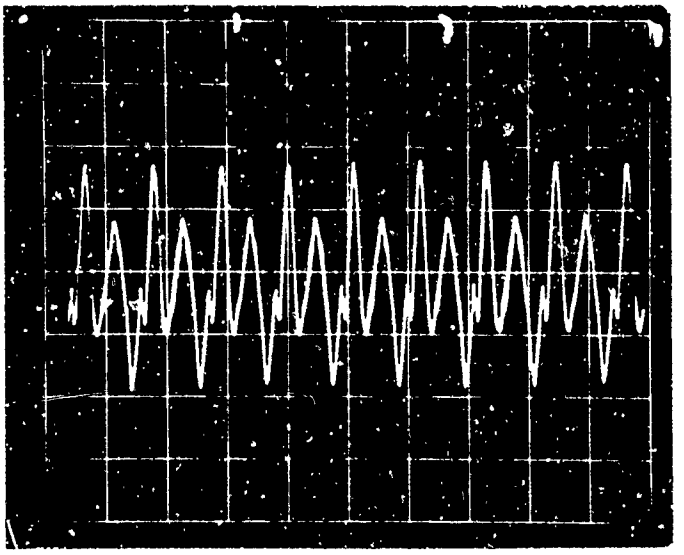

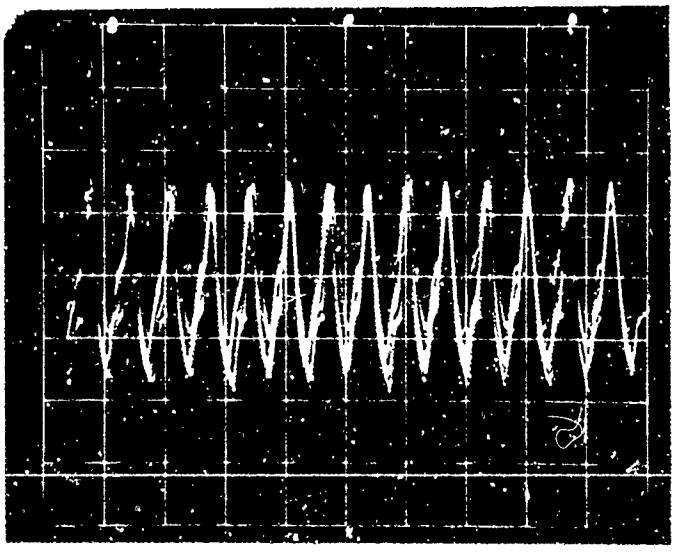

Figure 3.5. Typical Cavitation Waveforms

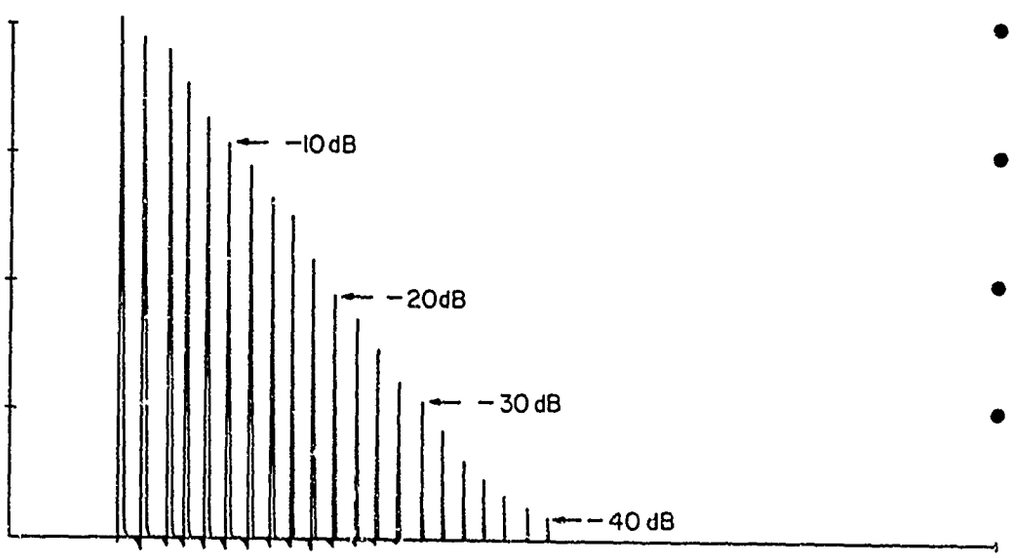

Figure 3.6. Calibration of X-Y Recorder

CHAPTER IV

THEORETICAL DISCUSSION

Numerous investigators have studied the general laws of cavitation inception and have derived simple and complex models that attempt to explain the physics involved. The equations of motion have been investigated by Noltingk, Neppiras, H. G. Flynn, and Blake, among others.[9, 10, 11] The purpose of this discussion is to list the basic equations that apply to cavitation phenomena and to apply the theoretical ideas to this investigation.

4.1 Cavitation Threshold

The following techniques are generally used to define cavitation threshold:

1. The appearance of a physical effect caused by cavitation,
2. The growth of the nuclei to a certain radius, and
3. The measurement of a certain amount of energy radiated by the collapsing cavities.

The resulting cavitation thresholds do not coincide. Cavitation threshold values are thus dependent on how the threshold is defined.

Various investigators have measured a line spectrum superimposed on a continuous spectrum and used the appearance of the line spectra as an indication of cavitation inception.[4] The spectrum is due to the following allowable cavity motion:[10]

1. Linear oscillations about the equilibrium radius,
2. Nonlinear oscillations about the equilibrium radius, and
3. Expansion of the cavity to a maximum size and its subsequent collapse and shock wave emission.

Typical radii versus time during collapse curves are very steep.[9] The pressure within the cavity and the wall velocity are very large during collapse.

Definite cavitation thresholds should be approached cautiously. The shape of the cavity interface during collapse is important and the size and distribution of nuclei is critical. The threshold will be frequency dependent whenever the forces are influenced by frequency. Esche's results show that cavitation threshold is independent of frequency for $f < 10^4$ Hz and dependent on frequency for $f > 10^4$ Hz.[4]

4.2 Bubble Dynamics

The equations of motion of a single isolated cavity will be developed by investigating the growth and collapse of the cavity when a sinusoidal driving force is applied. Since acoustic cavitation deals with the motions of these cavities,

it is important that the theoretical discussion be complete. The following approximations will be made:

1. The cavity has spherical symmetry,
2. The gas and vapor inside the cavity behave like an ideal gas,
3. The vapor pressure of the liquid inside the cavity is a constant,
4. The viscosity of the water will be neglected, and
5. The liquid is incompressible.

It is assumed that the cavity does not burst into a number of smaller bubbles when it collapses. Strasberg has shown that nuclei must exist in tap water for cavitation to occur at moderate driving amplitudes.[11] We will assume the existence of these nuclei.

Let a cavity with radius R_o be initially in equilibrium at $t = 0$ at a static pressure of $(P_L)_{t=0}$. The gas pressure inside the bubble at any R will be:

$$P_g(R) = P_g(R_o) \cdot \left\{\frac{R_o}{R}\right\}^{3\gamma} . \qquad (4.1)$$

The ratio of specific heat γ is equal to one for the isothermal case, and $P_g(R_o)$ is the gas pressure in the cavity at $t = 0$. Then,

$$P_g(R) = P_g(R_o) \left\{\frac{R_o}{R}\right\}^{3} , \qquad (4.2)$$

and the condition for stable equilibrium at $t = 0$ is:

$$P_g(R_o) + P_v = \frac{2\sigma}{R_o} + (P_L)_{t=0} , \tag{4.3}$$

where P_v is the vapor pressure, and σ is the surface tension.

Changing the static pressure to P_L, the condition for equilibrium at the new radius R is:

$$P_g(R_o) \left\{\frac{R_o}{R}\right\}^3 + P_v = \frac{2\sigma}{R} + P_L . \tag{4.4}$$

The new equilibrium radius is determined from Equation (4.4).

When $P_L < P_v$, the cavity will be in stable equilibrium only if its radius is less than a critical radius R_c, where

$$R_c = \frac{4\sigma}{3|P_L - P_v|} . \tag{4.5}$$

If $R > R_c$, the cavity will expand to a maximum value.[10]

The Noltingk-Neppiras equation of motion for a single cavity in an incompressible liquid is derived by equating the total work done by forces acting on the bubble to the total kinetic energy and differentiating the resulting energy equation. The equation of motion for growth of a single cavity is:

$$\ddot{R}R + \frac{3}{2}\dot{R}^2 = \frac{P_L(t) - P_\infty(t)}{\rho} , \tag{4.6}$$

where ρ is the constant density of the liquid and P_∞ is the pressure in the liquid at large distances from the cavity wall. Using the equilibrium equation for a stable cavity for the isothermal case, we have:

$$P_L(t) - P_\infty(t) = P_g(R_o)\left(\frac{R_o}{R}\right)^3 + P_v - \frac{2\sigma}{R} - (P_L)_{t=0} , \qquad (4.7)$$

where

$$P_\infty(t) = (P_L)_{t=0} .$$

If we include a sinusoidal driving force $P_A \sin \omega t$, Equation (4.6) becomes:

$$\ddot{R}R + \frac{3}{2}\dot{R}^2 = \frac{P_g(R_o)\left(\frac{R_o}{R}\right)^3 + P_v + P_A \sin \omega t - \frac{2\sigma}{R} - (P_L)_{t=0}}{\rho} . \qquad (4.8)$$

It is difficult to find a general solution to Equation (4.8). Noltingk and Neppiras used a digital analyzer to obtain specific solutions for different system conditions. Their results show that $\dot{R}$ becomes extremely large for small R during collapse.

For small $\frac{\dot{R}}{v_s}$, the Rayleigh solution at constant P_∞ and constant pressure within the cavity is:

$$(\dot{R})^2 = \frac{2}{3}\left|\frac{(P_L)_{t=0} - P_c}{\rho}\right|\left[\left(\frac{R_o}{R}\right)^3 - 1\right] , \qquad (4.9)$$

where P_c is the pressure within the cavity.

The time t required for this cavity to collapse is:[10]

$$t = 0.915\, R_{max} \sqrt{\frac{\rho}{(P_L)_{t=0} - P_c}} \quad , \tag{4.10}$$

where R_{max} is the size of cavity when it begins to collapse.

Boguslawskii's solution[12] is:

$$(\dot{R})^2 = \frac{2}{3} \frac{(P_L)_{t=0} - P_v + \frac{2\sigma}{R}}{\rho} \left(\frac{R_o}{R}\right)^3 \ln\left(\frac{R}{R_o}\right)^3 + \frac{2}{3} \frac{P_A + P_v - (P_L)_{t=0}}{\rho} \left[1 - \left(\frac{R_o}{R}\right)^3\right] \frac{-2\sigma}{R} \left[1 - \left(\frac{R_o}{R}\right)^2\right] , \tag{4.11}$$

and the time required for the cavity to collapse is:

$$t = \bar{R} \sqrt{\frac{3}{2} \frac{\rho}{\left[P_A + P_v - (P_L)_{t=0}\right]}} \quad , \tag{4.12}$$

where $\bar{R}$ is the average radius.

4.3 Subharmonic Generation

The existence of subharmonic oscillations has been discussed by H. G. Flynn.[10] He obtained a linear equation from the general Noltingk-Neppiras equation and discussed the periodic solutions. Flynn's procedure was the following:

1. Let $R = R_o + r$ for $r \ll R_o$,
2. Expand $\left(\frac{1}{R}\right)$ by a Taylor series in r about R_o , and
3. Neglect the nonlinear terms when the result is substituted into Equation (4.6).

The linear equation for the isothermal case is:

$$\ddot{r} + \omega_o r = \frac{P_A}{\rho R_o} \sin \omega t \ , \tag{4.13}$$

where the linear resonant frequency ω_o is determined by:

$$\omega_o^2 = \frac{1}{R_o^2 \rho} \left[\left((P_L)_{t=0} + \frac{2\sigma}{R_o} - P_v \right) - \frac{2\sigma}{R_o} \right] . \tag{4.14}$$

The cavity will oscillate linearly with increasing amplitude at this frequency.

If we impose the initial condition that

$$\dot{R} = 0 \text{ at } t = 0 \ , \tag{4.15}$$

the following two solutions result:

when $(\omega = \omega_o)$,

$$r = \frac{P_A}{2\rho R_o \omega_o^2} \left[\sin \omega_o t - \omega_o t \cos \omega_o t \right] ; \tag{4.16}$$

when $(\omega \neq \omega_o)$,

$$r = \frac{P_A}{\rho R_o(\omega_o^2 - \omega^2)} \left[\sin \omega t - \left(\frac{\omega}{\omega_o} \right) \sin \omega_o t \right] ; \qquad (4.17)$$

or $$r = A(\omega) \sin \omega t + B(\omega) \sin \omega_o t . \qquad (4.18)$$

Two oscillations exist for $\omega \neq \omega_o$. Flynn calls these oscillations forced and free oscillations, respectively. The free oscillation has a characteristic frequency ω_f $(\omega_f \neq \omega_o)$. The condition for periodicity of the nonlinear motion is then:

$$\frac{\omega}{\omega_f} = \frac{n}{m} ; \frac{n}{m} \text{ is a rational number.} \qquad (4.19)$$

The result may be summarized by the following:

1. Subharmonics exist when $m = 1$ and $n > 1$.
2. Harmonic components exist whenever $n = 1$ and $m > 1$.

CHAPTER V

EXPERIMENTAL RESULTS

5.1 Measurements of the Anechoic Tank

Tests were made to determine how much the tank distorted the acoustic field for the two frequencies that were used throughout the investigation. The 4X-47 projector was placed at the bottom of the tank and the deviation from inverse square law behavior was obtained by fixing the position of the projector and using 2-inch interval increments for the LC-5 receiver. Data was taken at a single frequency for intermediate plate current (200 ma). A typical result is shown in Figure 5.1. The straight line represents 6 dB per octave transmission loss expected for inverse square loss behavior. It is apparent that the signal is propagated for small transducer-receiver separations as if the source emits a plane wave. For separations greater than 6-inches, the spherical transmission law is obeyed. The scattering in data about the 6-inch reference line is due to reflections and variation of projector pattern with frequency.

Under exactly the same conditions as above, a check was made to find out how the intensity of the applied field influenced transmission in the anechoic tank. Data was obtained at three

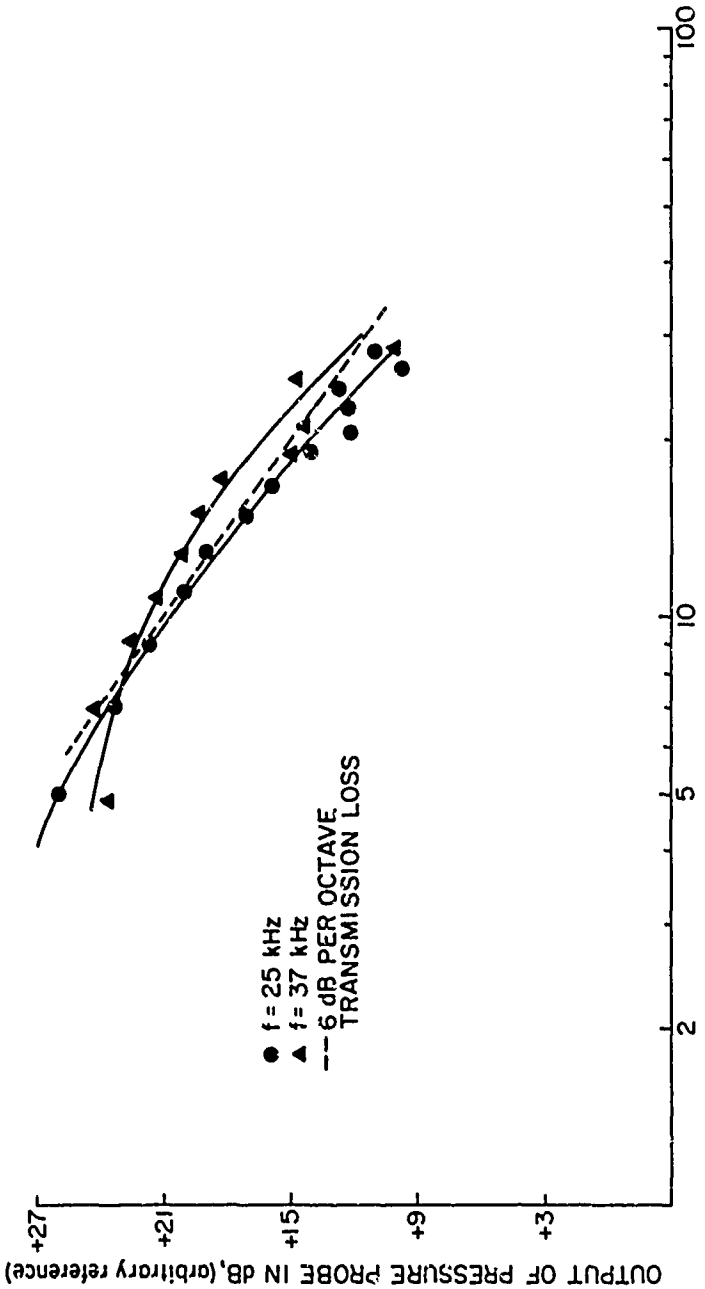

Figure 5.1. Output of the Pressure Probe at Two Frequencies

driving voltages at 31.8 kHz and is shown in Figure 5.2. The straight line again represents 6 dB per octave transmission loss using the 10-inch data point as the reference. It is apparent that intensity influences inverse square behavior either by affecting the pattern or by an increase in reflections.

Tests were taken to find the useful frequency range of the four-foot long, three-foot wide, and two-foot deep fir-lined tank. Pulses of short duration were used to lower interference in the tank. Continuous wave testing was avoided due to the consequent high reflected pressure pulses. The pressure pulses were picked up by the LC-5 hydrophone and displayed on the oscilloscope. The position of the QP-1 transducer was fixed and measurements were made with the tank top off. The LC-5 hydrophone was placed at separations of 16 and 30 inches to show the influence of the boundaries. Typical oscillograms with and without the tank top, at different separations, are shown in Figures 3.2 and 3.3. To check how the results depended on the position of the transducer and receiver and what influence the top had, tests were taken with the tank top on at two separations. The projector was placed on the bottom and also near the surface. The results are shown in Figures 5.3, 5.4, and 5.5. The data show that the wedges absorb better than 95 percent of the direct energy for frequencies from 30 to 110 kHz. No data was taken below 25 kHz due to the dimensions

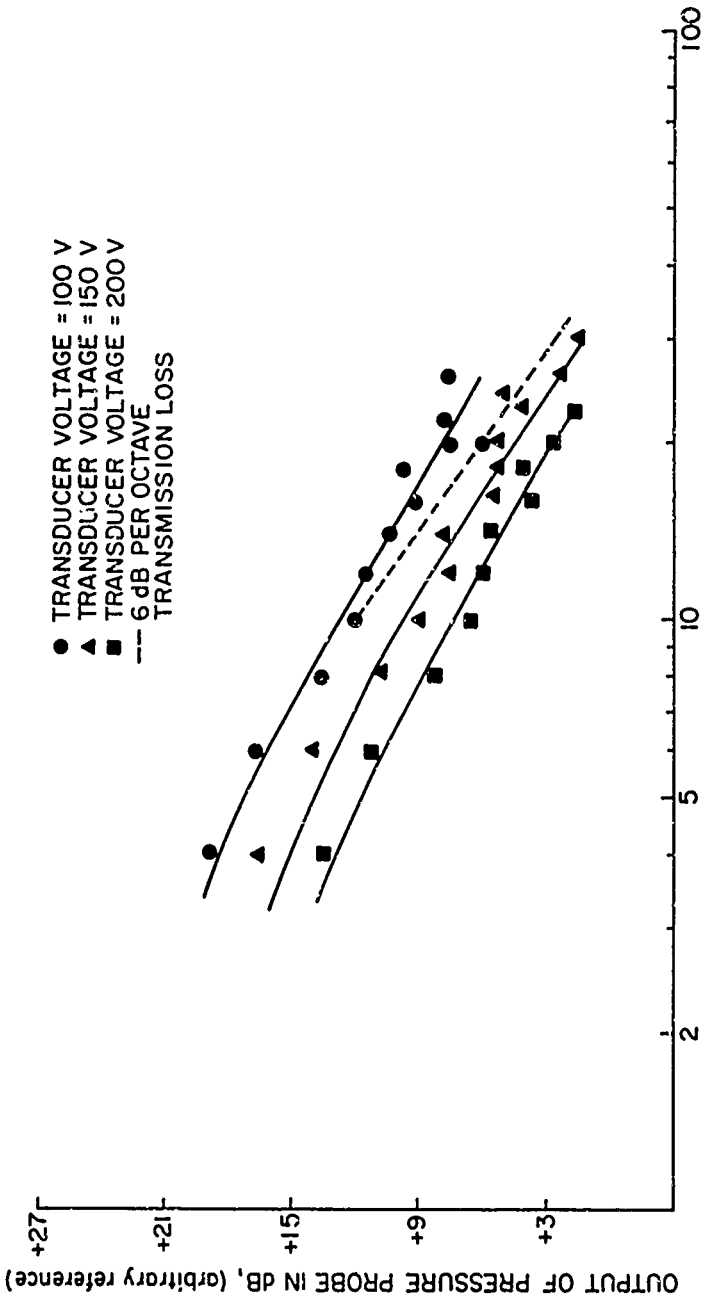

Figure 5.2. Output of Pressure Probe for Different Driving Voltages

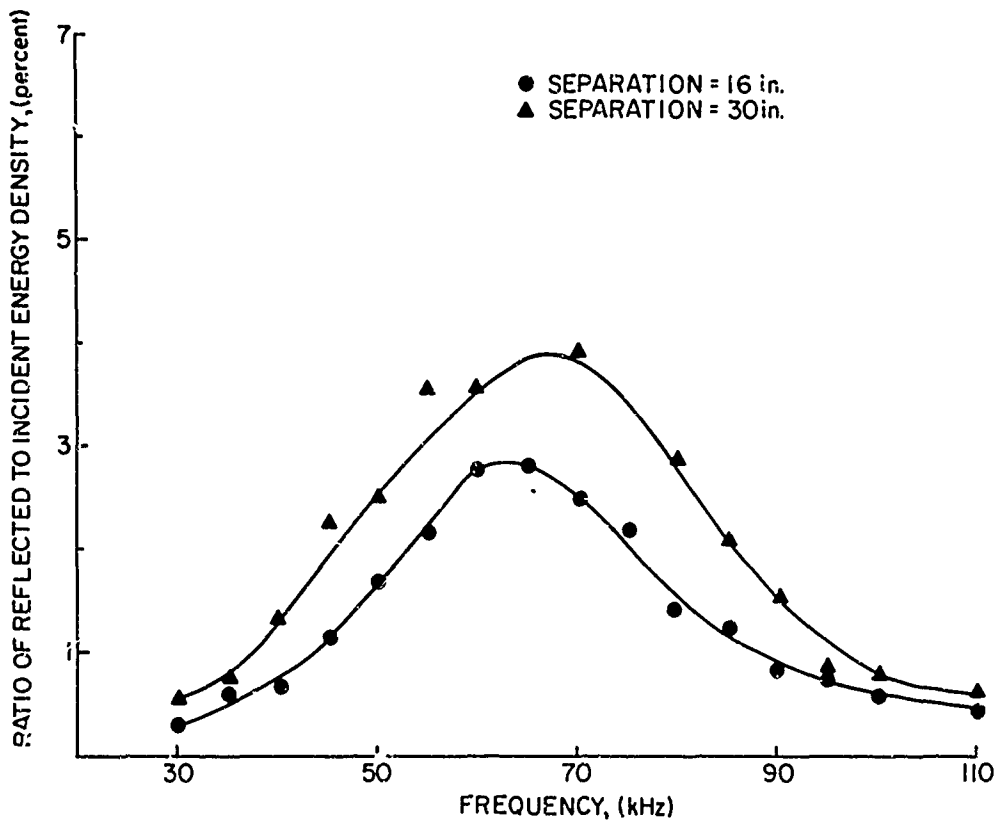

Figure 5.3. Ratio of Reflected to Incident Energy Density with Projector on the Bottom and Top On

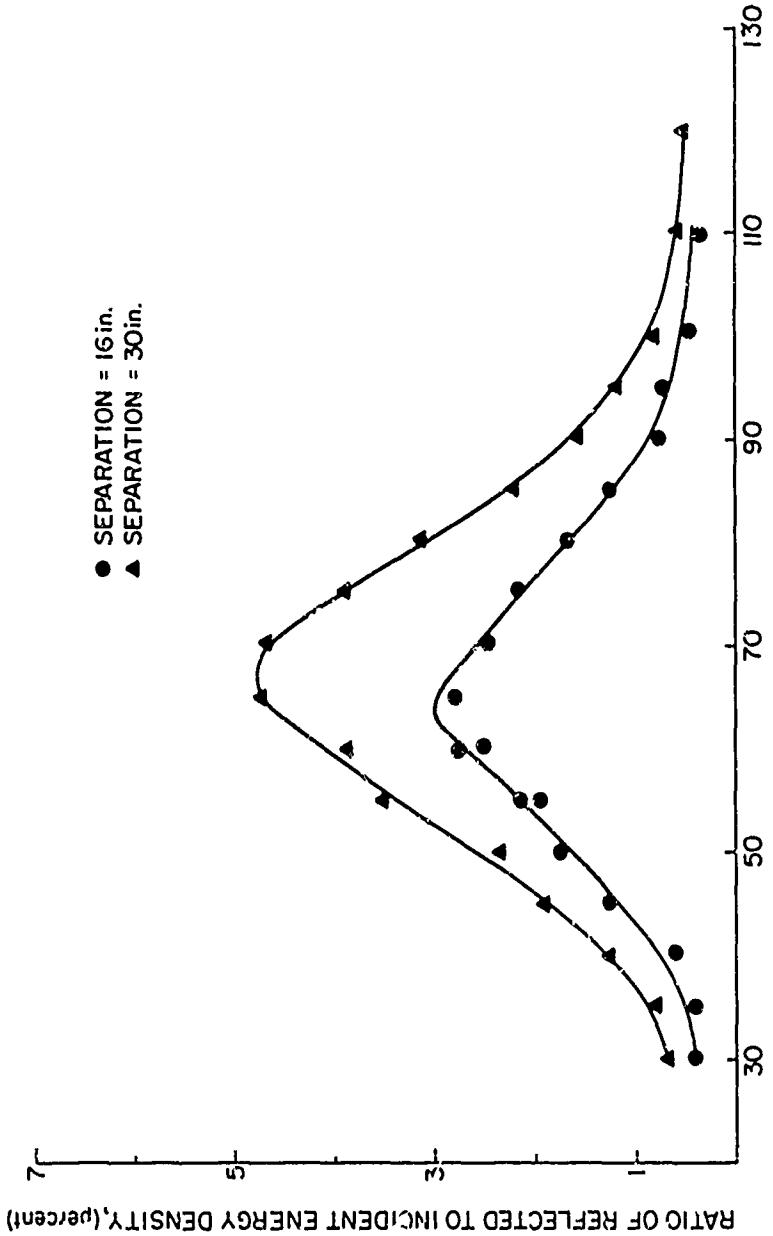

Figure 5.4. Ratio of Reflected to Incident Energy Density with Projector on the Bottom and Top Off

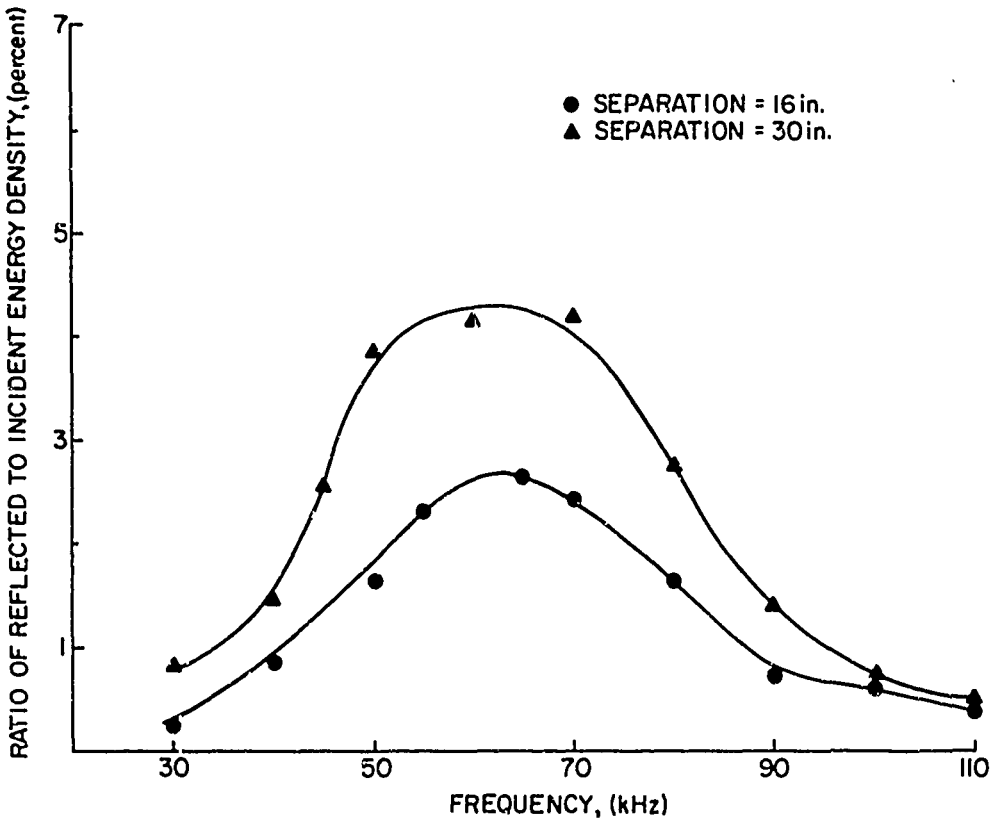

Figure 5.5. Ratio of Reflected to Incident Energy Density with Projector Near the Surface and Top Off

of the tank. A maximum occurs for all three conditions at 65 kHz. This is due to existing standing waves and a particular dimension of either the wedges or the tank. The maximum in reflected energy is not due to projector pattern variations, for it occurs at both separations.

The anechoic tank is a definite improvement over the 5-1/2 gallon glass tank although it does not offer true free-field conditions. Unfortunately, no real comparison could be made between the two tanks due to their different dimensions and volumes. No comparison was made between the lined and unlined anechoic tank due to the time limit of this investigation.

5.2 Measurements of the 4X-47 Transducer

As stated in the scope of the investigation, the basic problem of this study was to develop a technique whereby the onset of cavitation could be determined easily and accurately. Distortion measurements proved to be good indicators of cavitation. The anechoic tank was built to reduce reflections of the direct energy pulses. It was felt that cavitation would dominate finite amplitude distortion for small distances in a semi-free-field medium. Power measurements of the transducer vibrating in the liquid medium were made. This involved measuring the complex electrical impedance $\overline{Z}$ of the 4X-47 transducer at and around its resonant frequency. Figure 5.6 shows the equivalent circuit of the 4X-47 transducer.

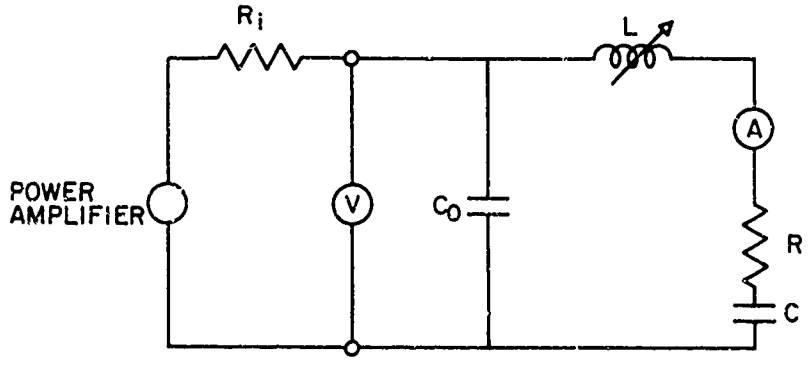

Figure 5.6. Equivalent Circuit of the 4X-47 Transducer

The insertions needed to measure the impedance magnitude at two resonant frequencies are also shown. The voltages and current values were both converted to effective values, and data was taken versus transducer voltage using

$$\left|\overline{Z}\right| = \frac{V \text{ volts (rms)}}{I \text{ amps (rms)}} .$$

Figure 5.7 shows two electrical impedance versus voltage curves. Cavitation occurred at a transducer voltage near 50 volts and the curves show sharp changes in impedance magnitude in this input region.

An AD-YU Electronics Phase Meter, Model 405, was used to measure the phase angle between transducer voltage and current at two frequencies. This phase angle δ should remain constant for various driving voltages if the power amplifier and transducer are linear and change abruptly when cavitation begins. A check was made on the amplifier response from 20 to 150 volts at two frequencies using a 230 ohm resistive load. The results in Figure 5.8 show that the McIntosh amplifier is linear from 20 to 150 volts and small variations in δ are due to $\pm 2^{o}$ sensitivity variation of the phase meter. Figure 5.9 shows phase angle measurements for the 4X-47 transducer. The phase angle changes sharply in the cavitation region for both frequencies.

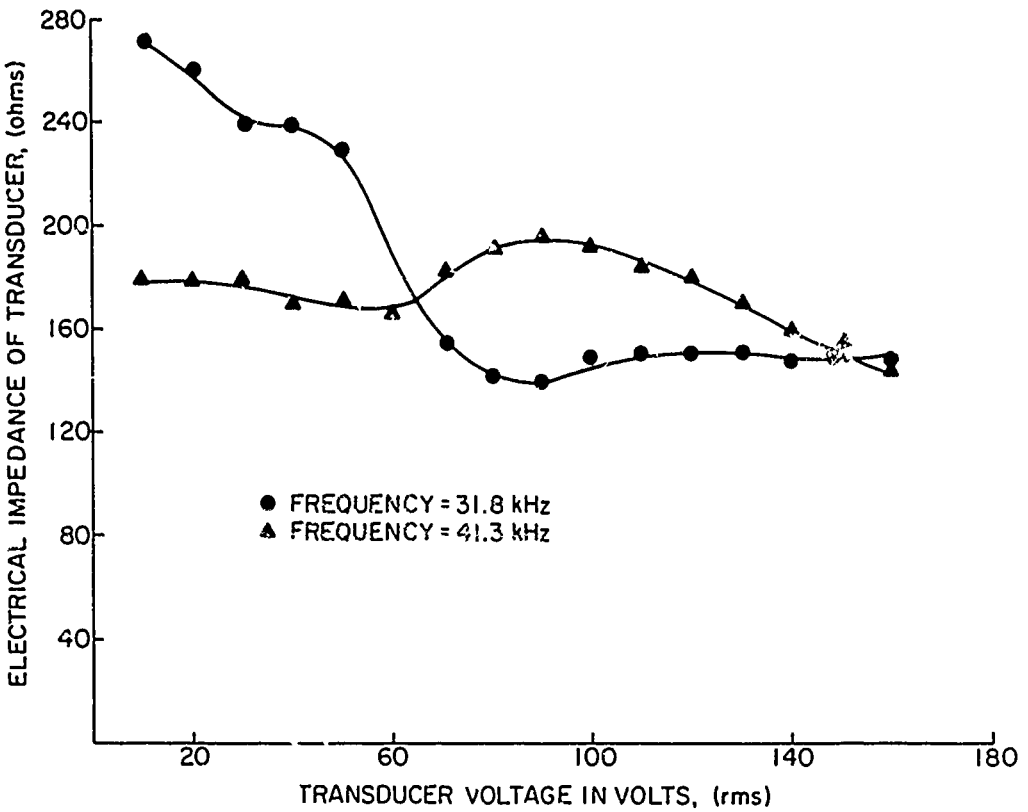

Figure 5.7. Electrical Impedance at Two Frequencies

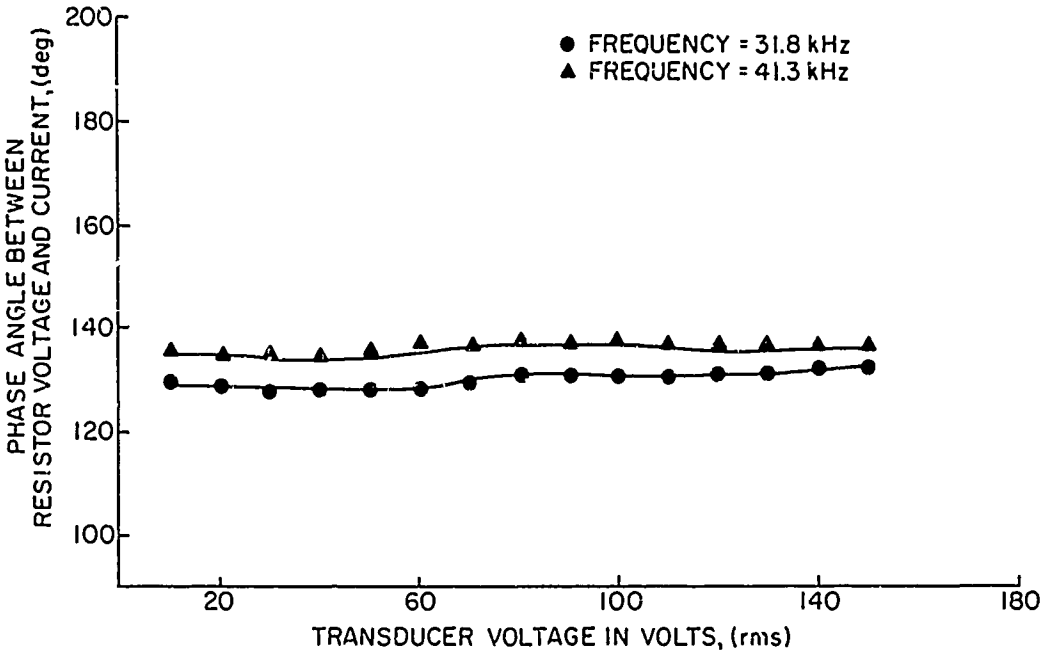

Figure 5.8. Phase Angle for a Resistive Load at Two Frequencies

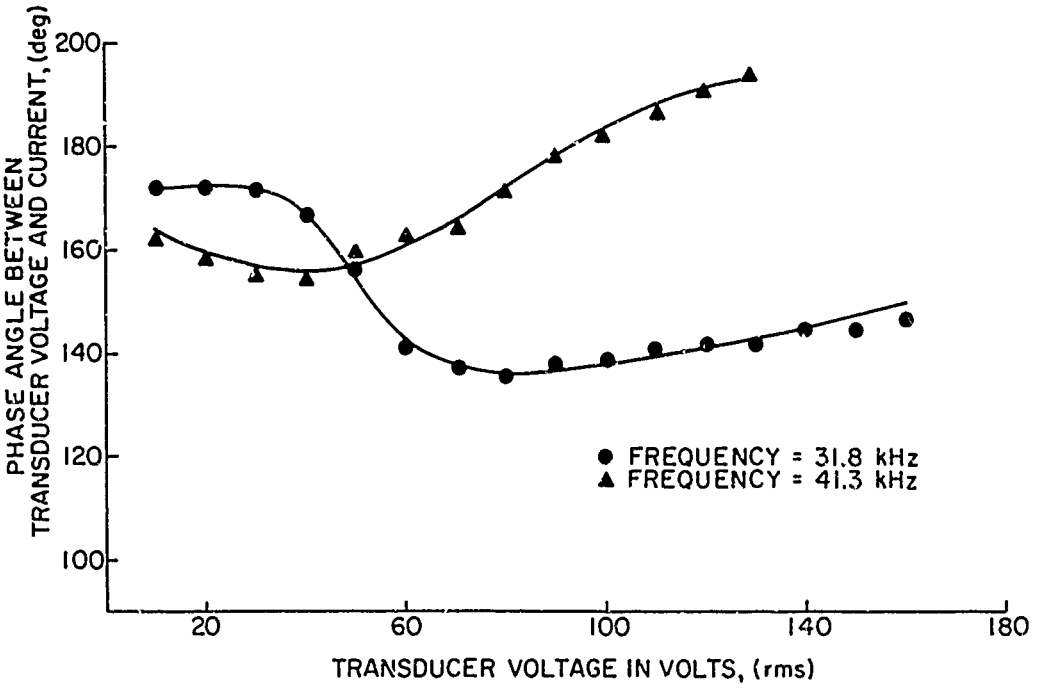

Figure 5.9. Phase Angle for the 4X-47 Load at Two Frequencies

Using

$$|R| = |\bar{Z}| \cos \delta$$

$$|X| = |\bar{Z}| \sin \delta ,$$

where R is the maximum electrical resistance, X is the maximum electrical reactance, and δ is the phase angle between transducer voltage and current, values of R and X were obtained for different transducer voltages. The results are shown in Figures 5.10 and 5.11 for two frequencies. The maximum resistance changes sharply at a transducer voltage of 50 volts rms and then levels off at larger transducer voltages for 31.8 kHz.

The previous results were combined to plot the complex transducer impedance at frequencies of 31.8 and 41.3 kHz for different transducer voltages. Figures 5.12 and 5.13 show the results. The circuit reactance of the transducer remains capacitive for 31.8 kHz over the 10 volt to 150 volt range. For 41.3 kHz, the reactance becomes inductive above 100 volts.

The pressure levels before and after cavitation at 15 inches are shown in Figure 5.14. The results are fairly linear for low inputs. Only small changes in the pressure level are evident during cavitation. The existence of weak cavitation does not contribute much to the overall intensity. It was believed that the resonant frequency of the transducer would change whenever cavitation sets in. This new resonant frequency

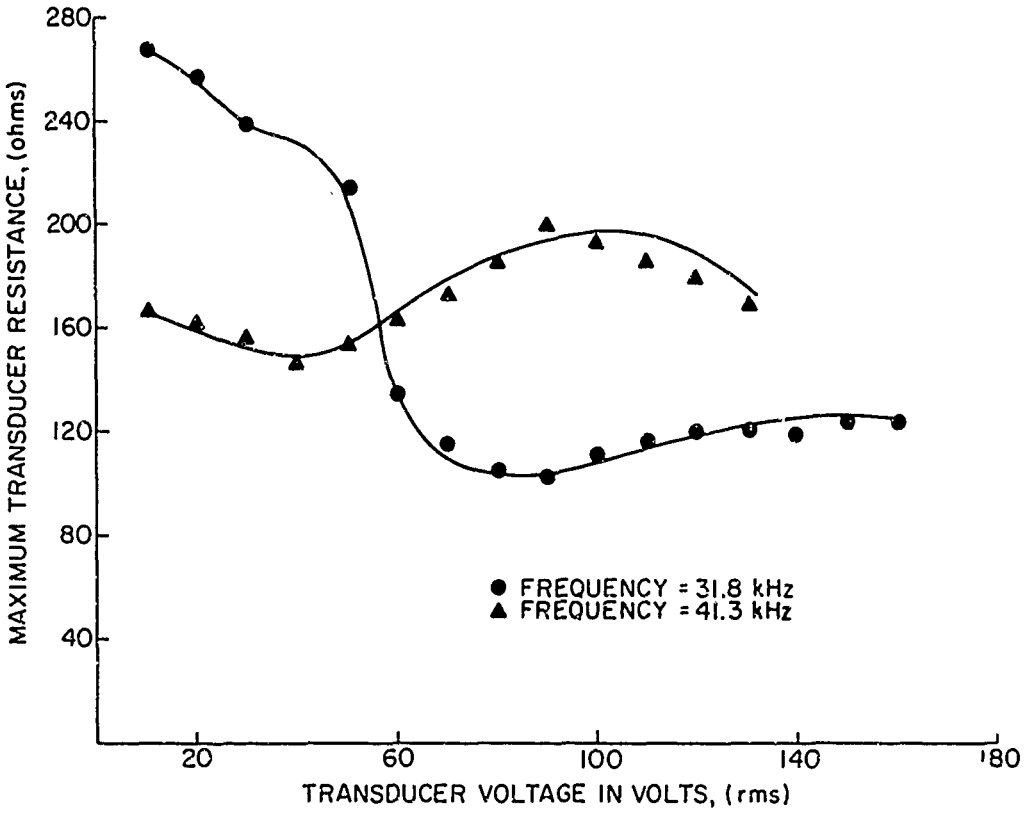

Figure 5.10. Transducer Resistance at Twc Frequencies

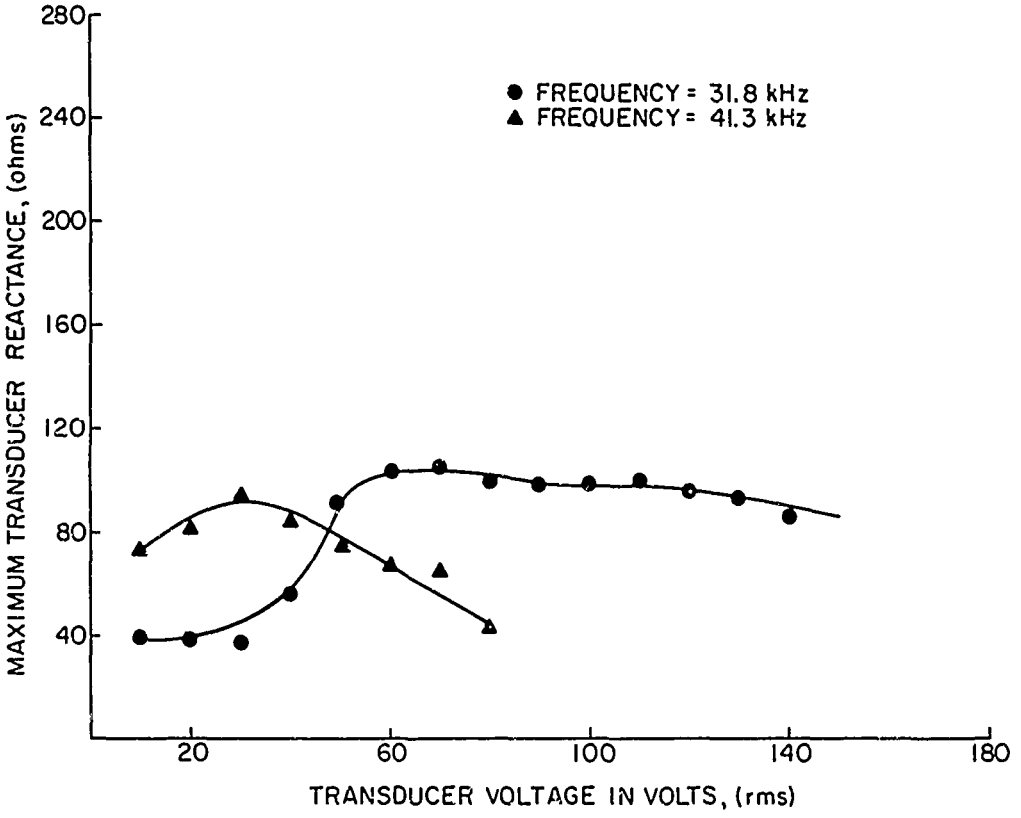

Figure 5.11. Transducer Reactance at Two Frequencies

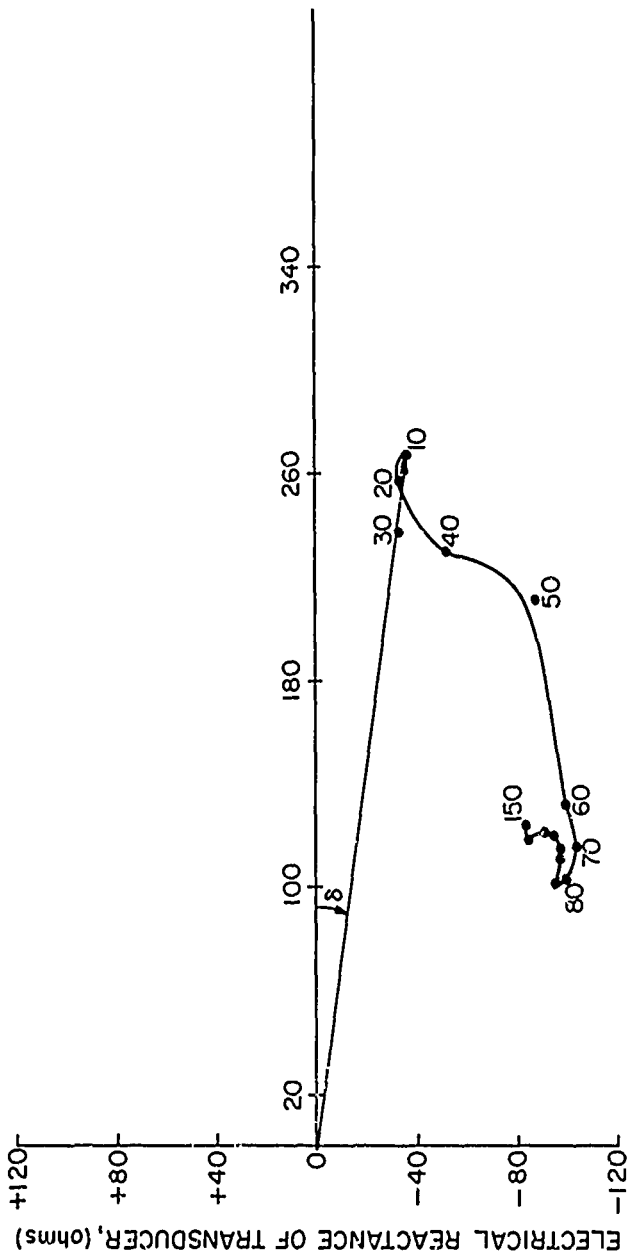

Figure 5.12. Electrical Transducer Impedance at 31.8 kHz

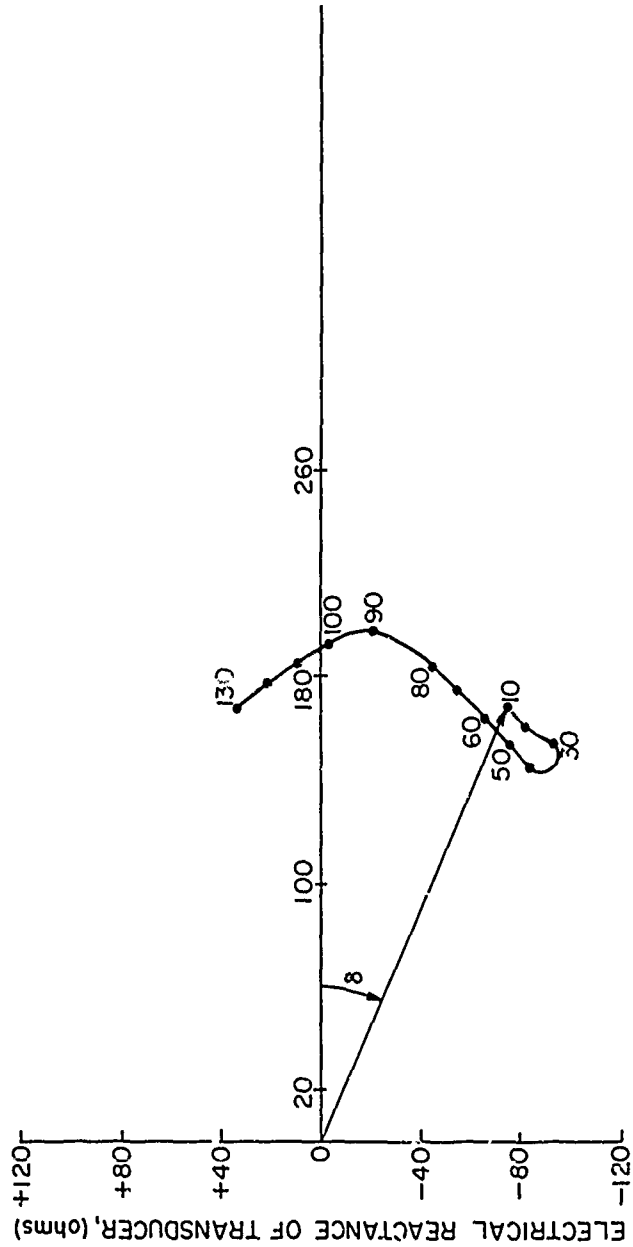

Figure 5.13. Electrical Transducer Impedance at 41.3 kHz

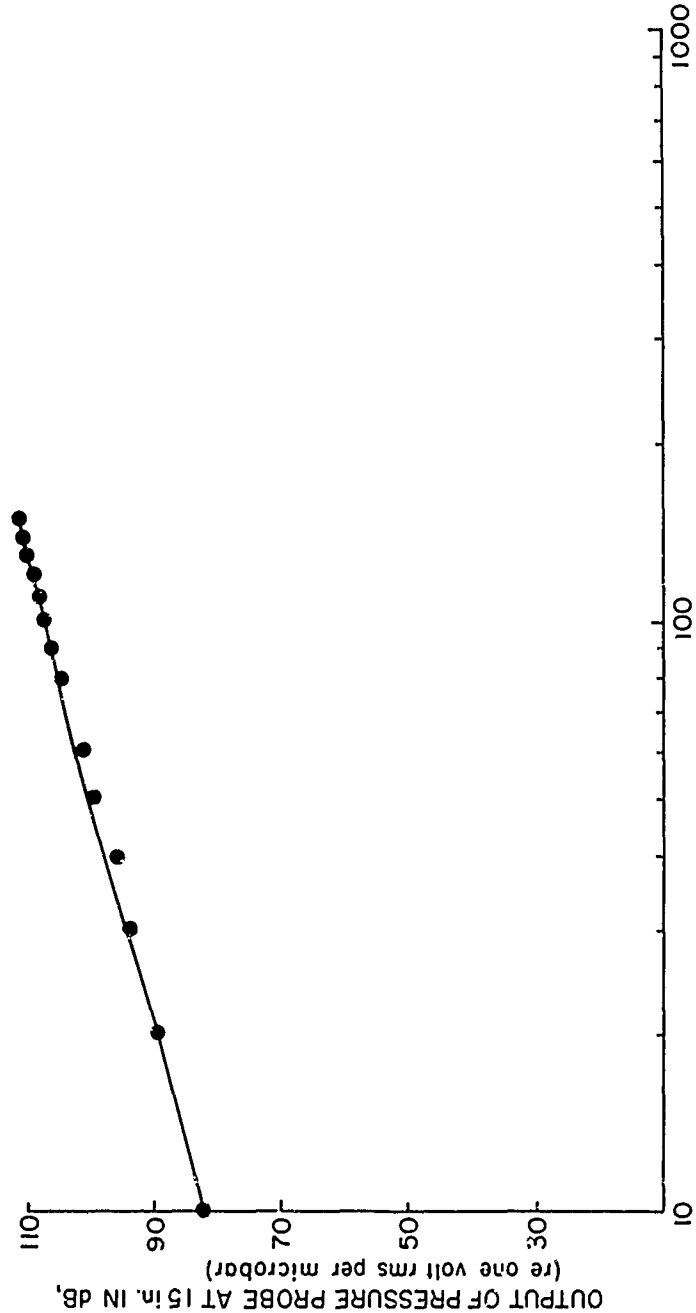

Figure 5.14. Output of the Pressure Probe at 32.3 kHz

is defined as that frequency which would give a maximum pressure probe output as the power input to the transducer is increased. Figure 5.15 shows that the pressure level again changes slowly and the results are fairly linear. Figure 5.16 gives the frequency of the maximum probe output as defined above. This resonant frequency is increased by almost 5 kHz in the cavitation region.

5.3 Total Harmonic Distortion Measurements

Total harmonic distortion measurements of the signal picked up by the LC-5 pressure probe using the 4X-47 projector were made with the Hewlett Packard distortion analyzer. The percentage of harmonic distortion is defined as:

$$THD_{\%} = 100 \times \left\{ \frac{E_2^2+E_3^2+E_4^2\ldots}{E_1^2+E_2^2+E_3^2+E_4^2\ldots} \right. ,$$

where, E_1 is the fundamental voltage, E_2 is the voltage of the second harmonic, and E_3 is the voltage of the third harmonic.

Harmonic distortion measurements require a pure-tone fundamental. A check was made of the amount of distortion introduced by the projector. Figures 5.17 and 5.18 show the percentage of harmonic distortion for the transducer voltage and current at two frequencies. The results show that, although the fundamental is not pure tone, the input side of the transducer has a negligible amount of distortion.

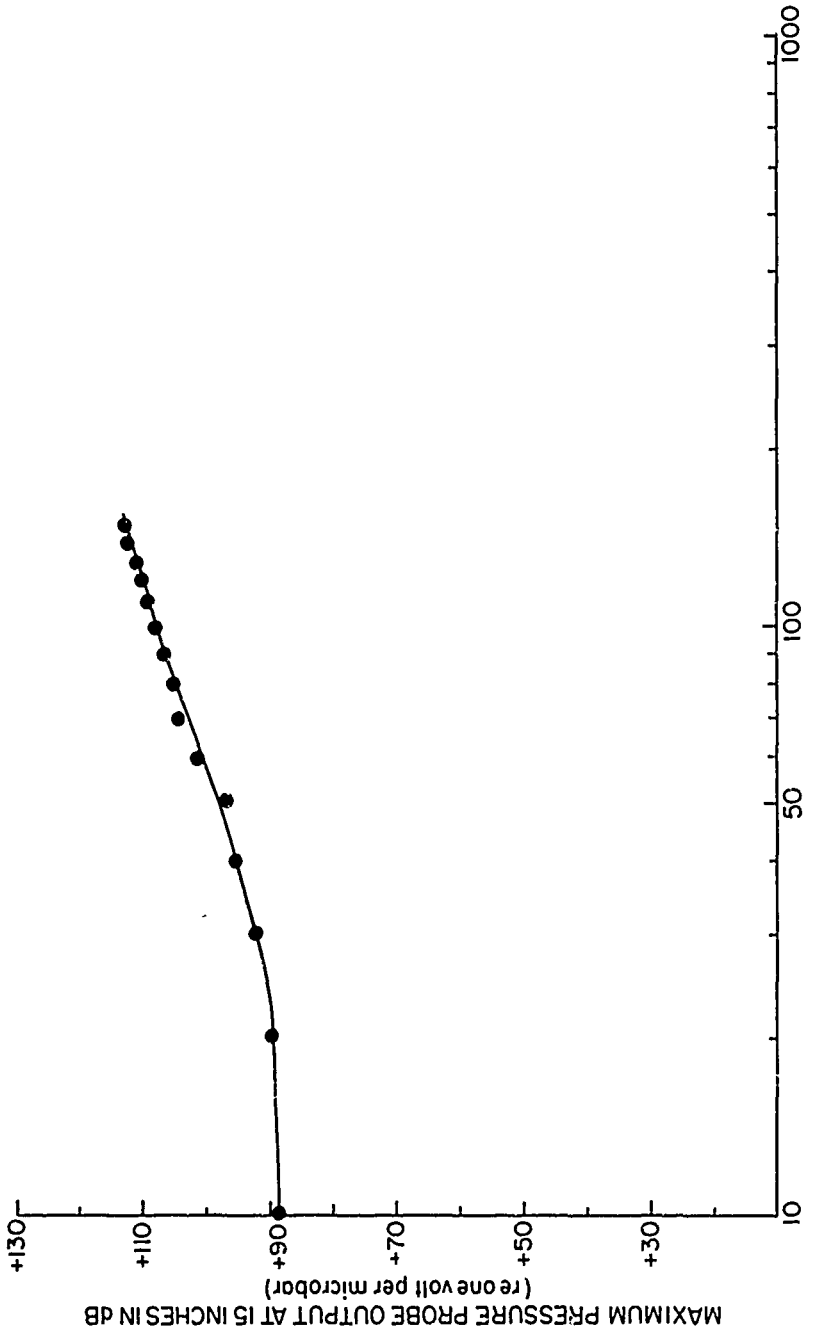

Figure 5.15. Maximum Output of Pressure Probe

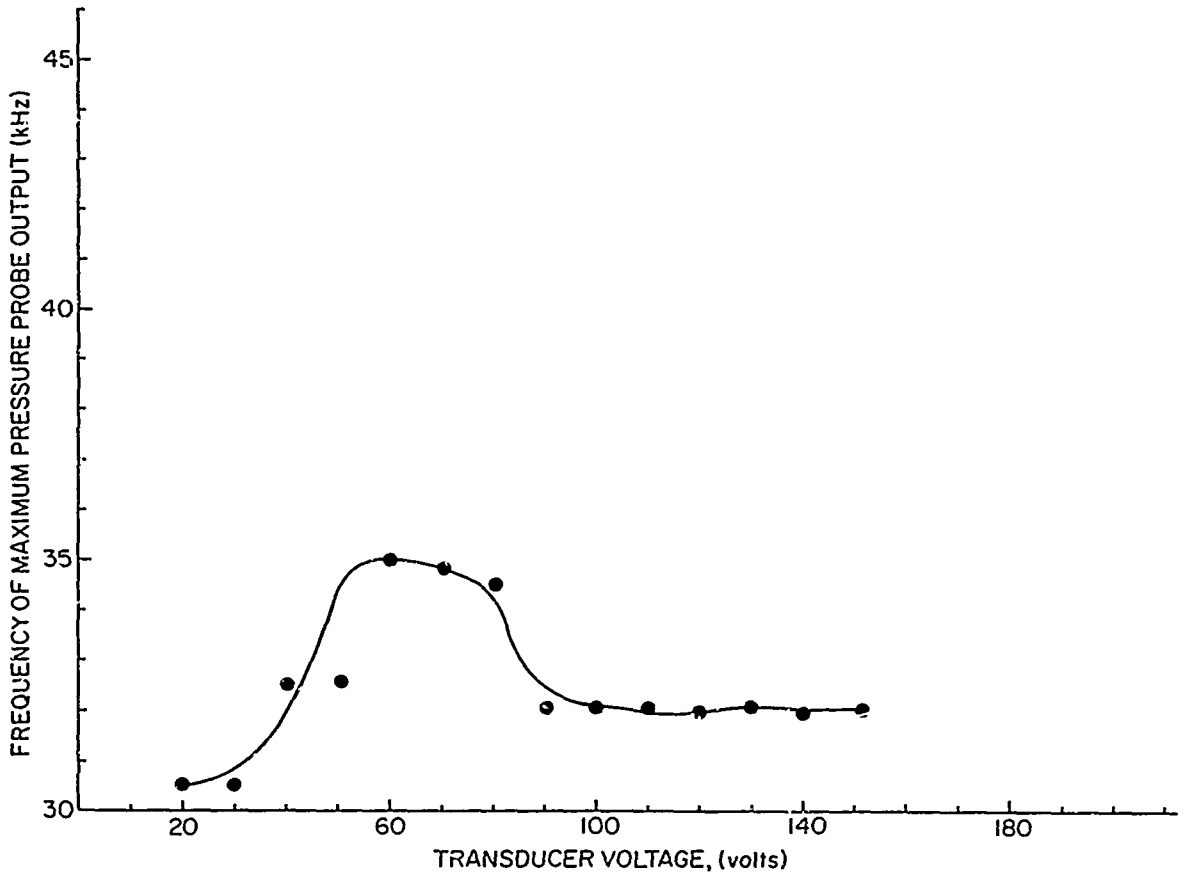

Figure 5.16. Frequency of Maximum Output of the Pressure Probe

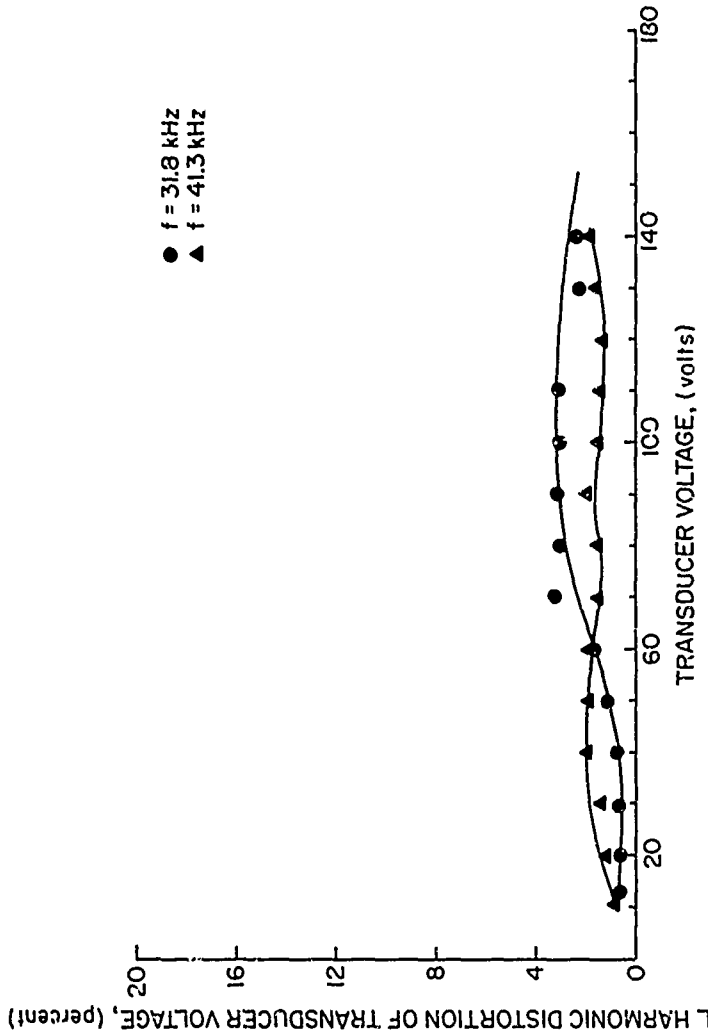

Figure 5.17. Total Harmonic Distortion of Transducer Voltage at Two Frequencies

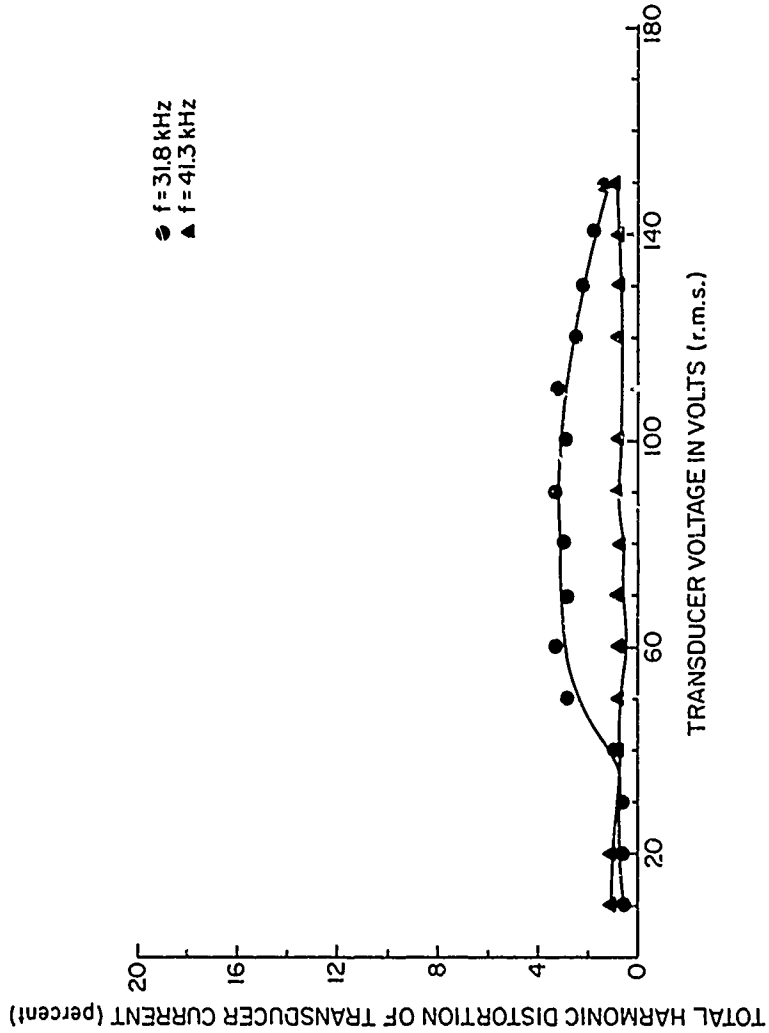

Figure 5.18. Total Harmonic Distortion of Transducer Current at Two Frequencies

The percentage of distortion of the probe output was measured at 31.8 kHz for separations of 16 and 30 inches. The preamplifier was not used in the measurements. Cavitation began at around 50 volts rms. The data in Figure 5.19 represent average readings. The distortion increased in the cavitation region and leveled off for input voltages greater than 120 volts. The results are independent of projector-receiver separation.

5.4 Spectrum Measurements

The line spectrum was investigated for various transducer voltages before and after cavitation. Figure 5.20 shows a typical variation of the fundamental amplitude for transducer voltages from 60 to 160 volts. Data was taken at separations of 5 and 15 inches for 41.3 kHz. The procedure is discussed in Chapter II, Section 4. A typical line spectrum plotted on the X-Y recorder is shown in Figure 5.21. Values of the second through fifth harmonic were measured and sharp changes in harmonic level were noted. The results are shown in Figures 5.22 through 5.25. Cavitation occurred at 50 volts. The level of the second through fifth harmonics are almost linear before and after the onset of cavitation. The pressure level of all of the harmonics does not increase after intense cavitation sets in.

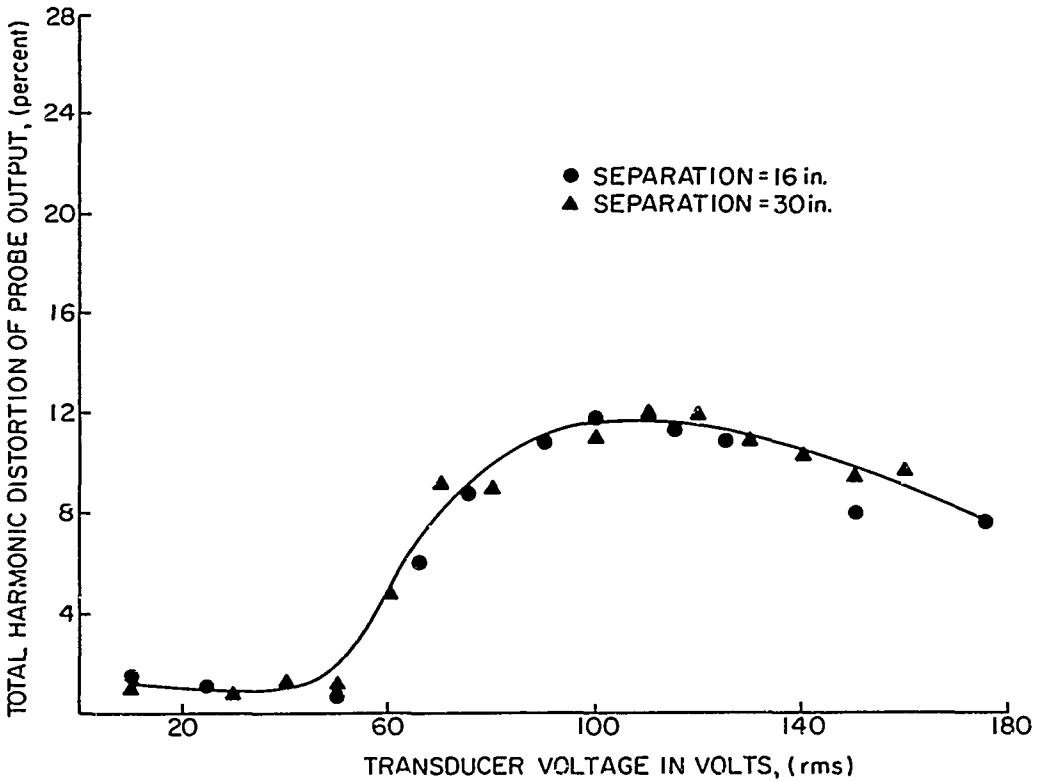

Figure 5.19. Total Harmonic Distortion of the Pressure Probe Output at Two Separations

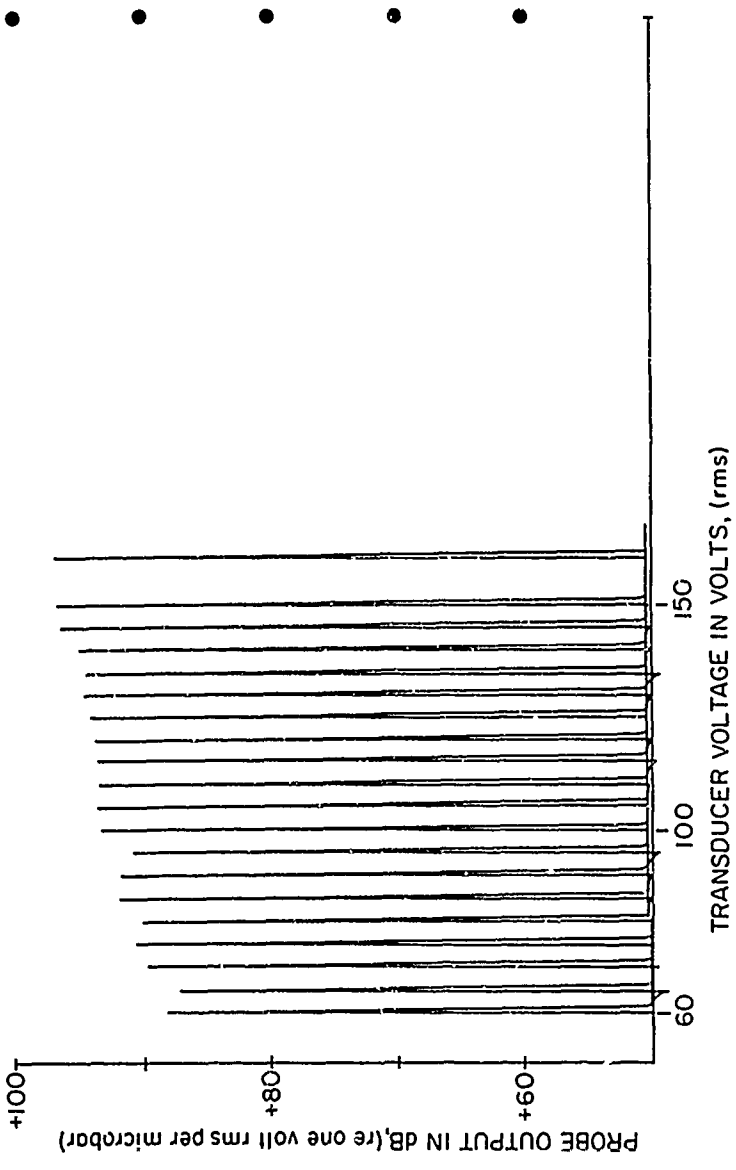

Figure 5.20. Typical Fundamental Voltage Variation

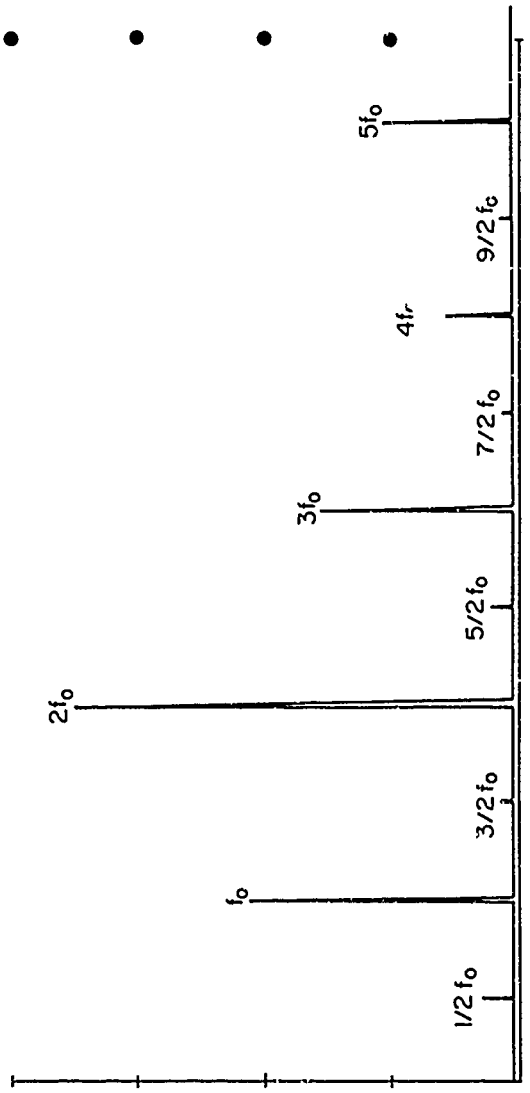

Figure 5.21. Typical Line Spectrum

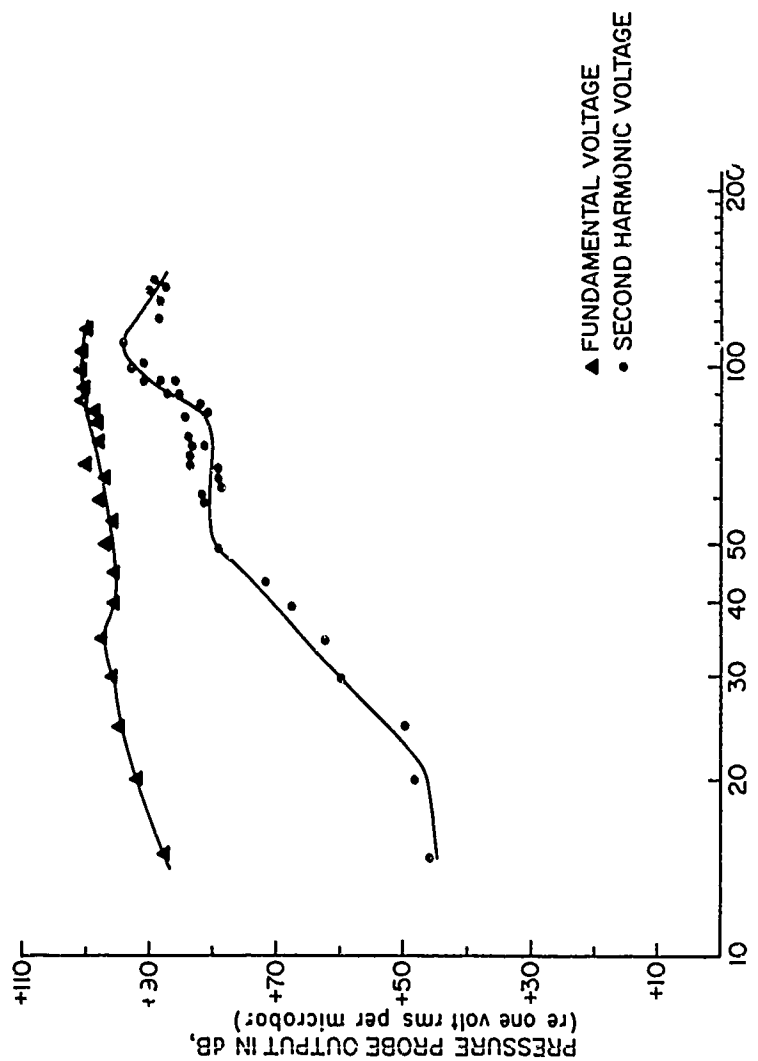

Figure 5.22. Second Harmonic as a Function of Transducer Voltage at a Transducer-Hydrophone Separation of 5 Inches

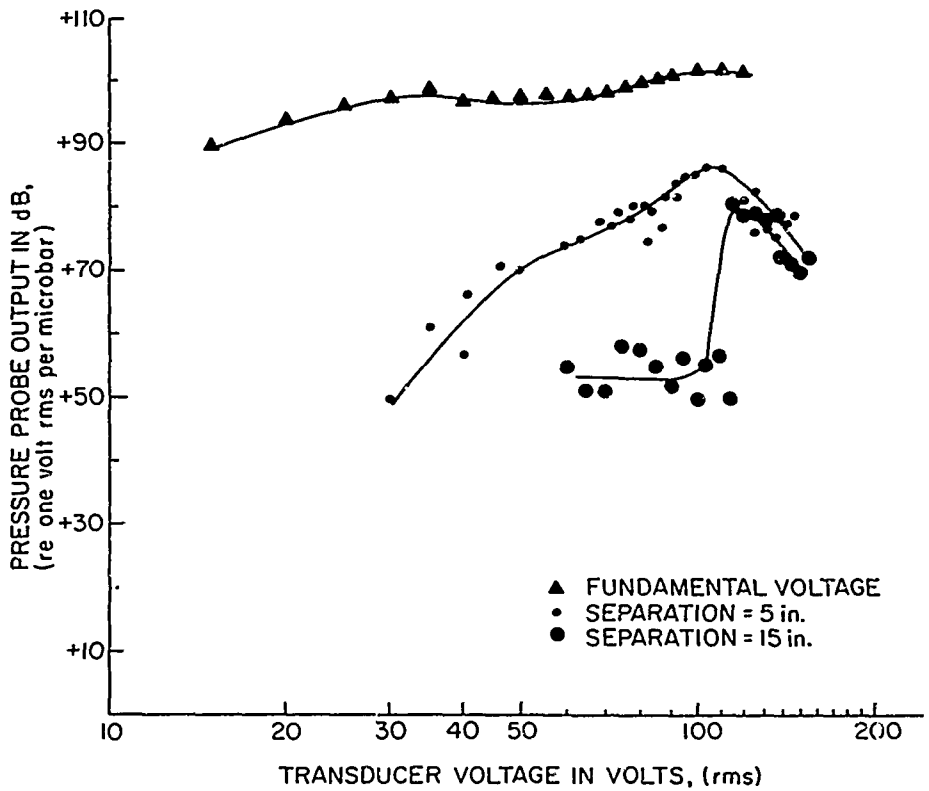

Figure 5.23. Third Harmonic at Two Transducer-Hydrophone Separations

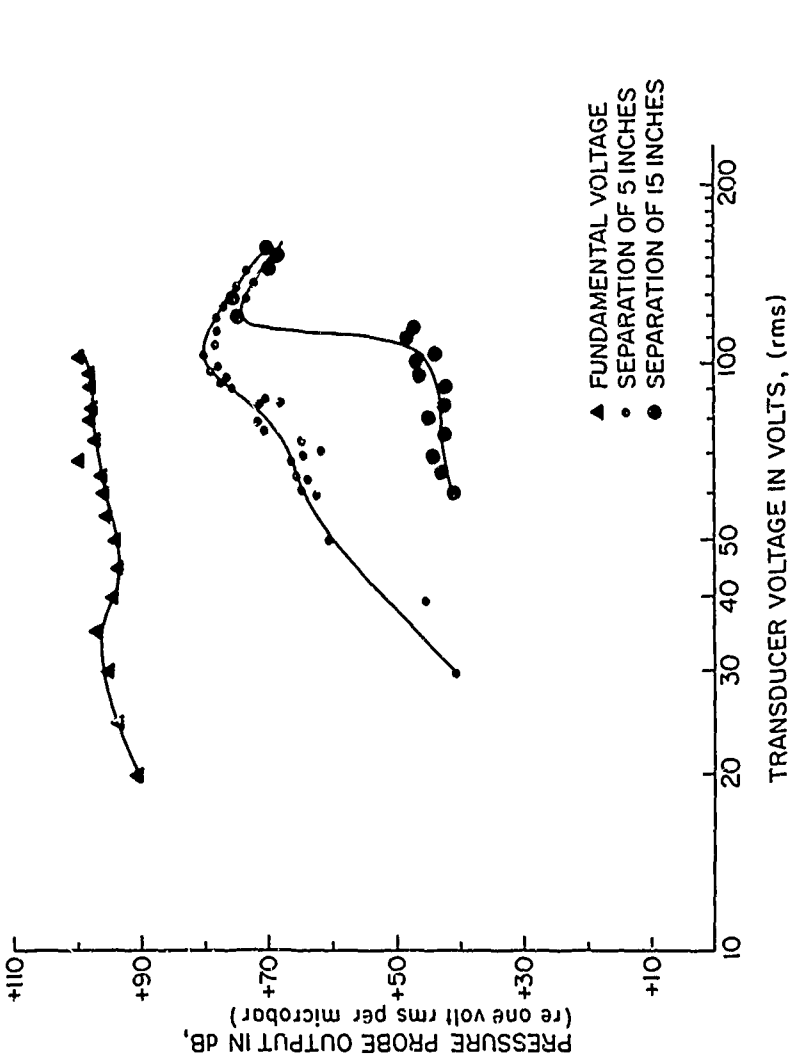

Figure 5.24. Fourth Harmonic at Two Transducer-Hydrophone Separations

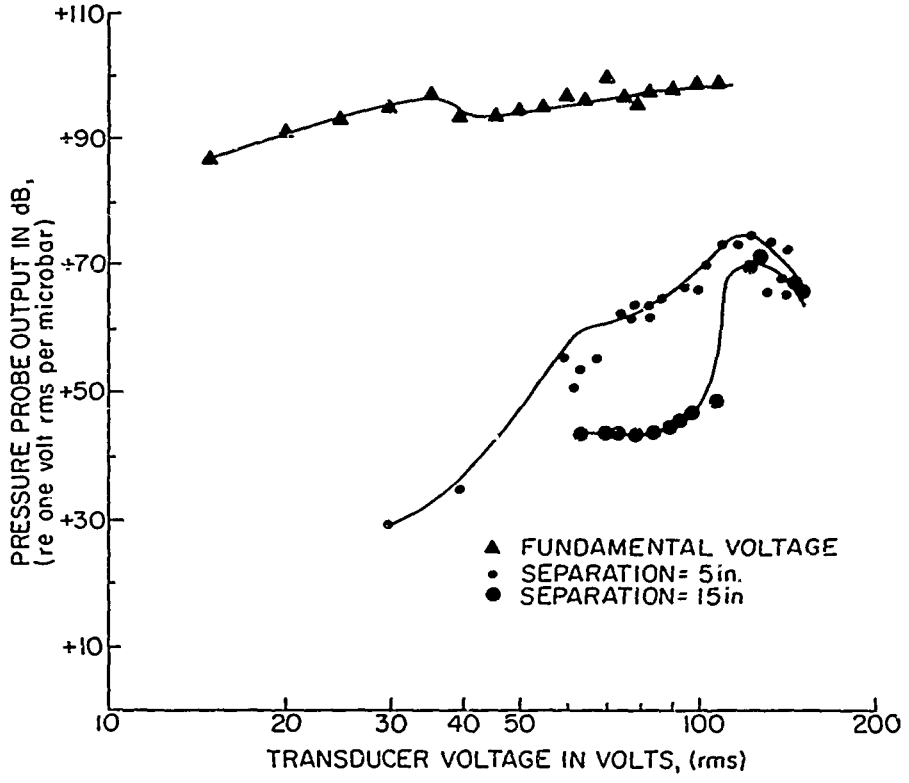

Figure 5.25. Fifth Harmonic at Two Transducer-Hydrophone Separations

CHAPTER VI

DISCUSSION OF THE RESULTS

Cavitation was defined to be the minimum pressure level that would raise the level of the second harmonic to within 15 dB of the fundamental. Cavitation in the anechoic tank began at a transducer voltage of 50 volts. This was verified by distortion measurements. The output waveform was displayed on the oscilloscope and the distortion was noted visually for increasing transducer voltages. The percentage of distortion, as measured by the distortion analyzer, was generally less than 1.5 percent for driving voltages less than 40 volts rms. At a transducer voltage of 50 volts, the distortion began to increase almost linearly and reached a value of 12 percent at 100 volts input. The distortion then leveled off to about 11 percent for higher transducer voltages.

The wide-band noise that is often used by observers to determine cavitation threshold was not detectable until the cavitation became intense at typical transducer voltages of 100 volts rms. Although the fundamental driving signal was filtered out and the remaining signals were increased by 40 dB,

the wide-band noise could not be heard at low cavitation intensities. Wide-band noise was heard only during intense cavitation.

The appearance of distortion due to cavitation proved to be a good indication of cavitation inception. Distortion set in suddenly as the transducer voltage was increased. A definite cavitation threshold did exist. Cavitation inception could also be defined in terms of the transducer voltage required to produce this large increase in distortion.

The output of the pressure probe was linear before and after cavitation. This surprising result can be explained if we assume that the transducer becomes partially unloaded when cavitation sets in. The appearance of vaporous bubbles makes the transducer operate as if it were in the air, with the result that it is no longer able to deliver increasing acoustic power with increasing transducer voltage. This condition also served as a good indication of cavitation.

The electrical properties of the transducer were expected to change due to the unloading effect. The best indication of an unloaded transducer would be the changing mass reactance that would result. The resonant frequency of the transducer would then change as the transducer voltage was increased. The new resonant frequency was defined as that frequency which would give a maximum pressure probe output at the higher transducer

voltage. The resonant frequency starts to increase at transducer voltages of 40 volts, reaches a broad maximum, levels off and remains at a higher value for large voltages. Since the waveform became distorted at a transducer voltage of 50 volts, this correlated well with the threshold criteria defined above. When the frequency was adjusted for maximum output, the output of the pressure probe was divided into two regions. A transducer voltage of 20 volts marked the deviation from linear output behavior.

The electrical properties of the transducer as a function of transducer voltage were further investigated by measuring the following:

1. The magnitude of the electrical impedance of the transducer.
2. The phase angle between transducer voltage and current.
3. The magnitude of electrical resistance of the transducer.
4. The magnitude of electrical reactance of the transducer.

The results proved to be frequency dependent. The frequency of 31.8 kHz was chosen from admittance measurements as a resonant frequency at low transducer voltages. The frequency of 41.8 kHz was not a resonant frequency at low

transducer voltages. Nevertheless, the transducer, when operated at the latter frequency, provided sufficient power output so that the electrical results could be examined for frequency dependency.

The electrical impedance and resistance both decrease sharply at a transducer voltage of 50 volts. The impedance slope is -7 ohms/volt when cavitation begins. The impedance then levels off to a value of 150 ohms with increasing transducer voltage. The electrical resistance slope is -6.2 ohms/volt at 50 volts input for 31.8 kHz.

As expected from the measurements of the changing resonant frequency mentioned earlier, the phase angle and the electrical reactance of the transducer both undergo changes at lower transducer voltages. The reactance begins to increase at 40 volts with a slope of +3.3 ohms/volt.

One can see that the results are frequency dependent. What we have really measured, of course, is the change in the resonant frequency of the transducer as the transducer voltage is increased. If we recall that only 31.8 kHz is a resonant frequency at low voltages, then different results can be expected if a non-resonant frequency is chosen at low input voltages and the frequency then adjusted for maximum transducer output.

The electrical measurements were verified by measuring the higher harmonics present when cavitation began. Of course, the spectrum measurements were used to determine the threshold in this

investigation. The effects on the spectrum due to cavitation were similar to those on the electrical measurements. The electrical changes that occur on the input side of the transducer correspond with the threshold as determined by the spectrum measurements. The second harmonic level was within 15 dB of the fundamental at a transducer voltage of 50 volts rms. The levels of the second through fifth harmonic level off after cavitation sets in. The second harmonic level is particularly constant immediately after cavitation. The slope of the second harmonic level changes abruptly at 50 volts.

The slope of the second harmonic level can give valuable information according to the following model of the kinetic motion of the cavitation nuclei. Cavitation is normally due to the underpressure amplitude. However, nuclei may also be formed through their kinetic motion. There exist two distinct cavitation regions. Microscopic cavitation may exist at small amplitudes where the nuclei have a Maxwell-Boltzman energy distribution. Liquids at room temperature have these microscopic regions that are capable of cavitating. Macroscopic cavitation is induced by large underpressure amplitudes.

A drastic boundary between microscopic and macroscopic cavitation does not exist. Cavitation is, therefore, a continuous process. The slope of the second harmonic level

in the microscopic region is determined by the Maxwell-Boltzman energy distribution. The sharp change of this slope marks the transition between microscopic and macroscopic cavitation.

Therefore, the second harmonic level yields valuable information. The slope of the second harmonic level can be used to measure the energy distribution of the nuclei and the nuclei content.

Thus, cavitation is a continuous process that starts at very small amplitudes. The intersection of the slopes of the second harmonic level in the microscopic and macroscopic regions should be determined and used to measure the threshold of cavitation.

This investigation has shown that the effects of cavitation are also excellent threshold criteria. The changes of the electrical impedance, resistance, reactance and the spectrum of the first few harmonics are particularly important. The effects are similar for low intensity cavitation at higher thresholds. A measurement of these effects would be a better measure of threshold than the commonly used wide-band noise criteria.

CHAPTER VII

SUMMARY

Acoustic cavitation was induced at frequencies of 31.8 and 41.3 kHz. The various tonpilz transducers and barium titanate disks were used as projectors. The anechoic tank built especially for this investigation had a capacity of 24 cubic feet. Tuning networks were built to increase the power radiated into the liquid. Measurements were made in a 5-1/2 gallon tank and the anechoic tank. The anechoic tank presented almost free-field measurement conditions.

The changes in the electrical side of the transducer were measured at transducer voltages before and after cavitation. The spectrum emitted at different transducer voltages was measured and the results were compared to the transducer measurements. The receiving hydrophone was calibrated up to 1 MHz at the Ordnance Research Laboratory of The Pennsylvania State University. The response of the hydrophone proved to be a practical indicator of spectrum level changes. The projector output was linear at all driving voltages. The unloading of the transducer, due to vaporous cavitation bubbles that appeared on its surface, was a good measure of

cavitation threshold. Cavitation threshold was defined as the minimum pressure level that would raise the level of the second harmonic to within 15 dB of the fundamental. Changes in electrical impedance, resistance, and reactance proved excellent indicators of cavitation threshold.

Higher harmonics were generated in the anechoic tank at low and high transducer voltages. The level of these harmonics changed at the onset of cavitation. The experimental results show that the pressure level of the first five harmonics was not increased greatly after cavitation. The level increased sharply before cavitation was established.

The onset of cavitation was determined by the change in the slope of the level of the second harmonic. Two distinct slopes of the second harmonic level existed. In the microscopic cavitation region, the slope was linear and the nuclei were formed by kinetic collisions. The slope changed abruptly when cavitation was induced by underpressure amplitudes.

It would be desirable to continue the study of the electrical properties of the input side of the transducer. More control of dissolved air in the liquid is required. The properties of the transducer in a pressurized liquid that is not capable of cavitating should be investigated and the results compared to those obtained in this investigation.

Low level half-order harmonics were present in this study. Unfortunately, their level was too low to be measured. The subharmonics were generated after the onset of cavitation. A spectrum analyzer with a 60 dB spread would be capable of measuring their level as a function of transducer voltage. The subharmonics were not as sensitive as the second harmonic in measuring the onset of cavitation.

BIBLIOGRAPHY

1. Blake, F. G., "The Onset of Cavitation in Liquids," Harvard University Acoustic Research Lab, Tech. Memo No. 11 (1949).

2. Noltingk, B. E., "The Effects of Intense Ultrasonics in Liquids," Handbuck der Physik, Vol. XI/2, Acoustics II, (Springer-Verlag, 1962).

3. Sette, D., "Effects of Solid Impurities on Cavitation Nuclei in Water," J. Acoust. Soc. Am., 41, (March 1967).

4. Esche, R., "Untersuchung der Schwingungskavitation in Flussigkeiten," Acustica, 2, Akust. Beih., AB 208 (1952).

5. Holak, W., "An Analysis of the Noise Spectrum Due to Cavitation Produced by Acoustic Fields," Ph.D. Thesis, The Pennsylvania State University (1956).

6. McDaniel, O. H., "Harmonic Distortion in Underwater Sound Projectors," The Pennsylvania State University, Ordnance Research Laboratory, Tech. Memo No. 302.2231-61 (1966).

7. Albers, V. M., Underwater Acoustics Handbook, (The Pennsylvania State University Press, 1960).

8. Darner, C. L., "An Underwater Sound Absorber for an Anechoic Tank," Underwater Sound Reference Laboratory Report No. 31 (1953).

9. Noltingk, B. E., and Neppiras, E. A., "Cavitation Produced by Ultrasonics," Proc. Phys. Soc., LXIV (1951).

10. Flynn, H. G., "Physics of Acoustic Cavitation in Liquids," Physical Acoustics, Vol. I, Part B, (Academic Press, 1964).

11. Strasberg, M., "Onset of Ultrasonic Cavitation in Tap Water," J. Acoust. Soc. Am., 31, (February 1959).

12. Boguslawskii, Y. Y., "Cavitation Threshold and its Frequency Dependence," Soviet Physics-Acoustics, 12, (April 1967).